ICP/EXT-04-00494

Fiscal Year 2004 Geostatistical Modeling of Lithologic Characteristics in the Radioactive Waste Management Complex for OU 7-13/14

Molly K. Leecaster

Idaho Completion Project

Bechtel BWXT Idaho, LLC

September 2004

ICP/EXT-04-00494
Project No. 23378

Fiscal Year 2004 Geostatistical Modeling of Lithologic Characteristics in the Radioactive Waste Management Complex for OU 7-13/14

Molly K. Leecaster

September 2004

Idaho Completion Project
Idaho Falls, Idaho 83415

Prepared for the
U.S. Department of Energy
Assistant Secretary for Environmental Management
Under DOE Idaho Operations Office
Contract DE-AC07-99ID13727

ABSTRACT

This report documents updated geostatistical modeling to predict lithology in the vadose zone beneath the Subsurface Disposal Area at the Radioactive Waste Management Complex at the Idaho National Engineering and Environmental Laboratory. Geostatistical modeling will improve the framework for hydrologic models that simulate fate and transport of groundwater and constituents carried by water. This work supports the remedial investigation and feasibility study for Waste Area Group 7 Operable Unit 7-13/14.

CONTENTS

FIGURES

TABLES

ACRONYMS

INEEL	Idaho National Engineering and Environmental Laboratory
MSE	mean square error
OU	operable unit
RI/FS	remedial investigation and feasibility study
RWMC	Radioactive Waste Management Complex
SDA	Subsurface Disposal Area
WAG	waste area group

Fiscal Year 2004 Geostatistical Modeling of Lithologic Characteristics in the Radioactive Waste Management Complex for OU 7-13/14

1. INTRODUCTION

This report documents updated geostatistical modeling to interpret lithology in the vadose zone beneath the Subsurface Disposal Area (SDA) at the Radioactive Waste Management Complex (RWMC) at the Idaho National Engineering and Environmental Laboratory (INEEL). Predictions in this report update previous predictions in *Geostatistic Modeling of Subsurface Characteristics in the Radioactive Waste Management Complex Region, Operable Unit 7-13/14* (hereinafter referred to as *Geostatistic Modeling in the RWMC Region*) (Leecaster 2002). Geostatistical modeling provides the geologic framework used in hydrologic models. Hydrologic models are important tools for predicting fate and transport of groundwater and the constituents carried by water. Understanding flow mechanisms is especially important for areas such as the SDA where hazardous constituents may move into groundwater. To apply deterministic hydrologic models, lithologic characteristics (i.e., the depth of subsurface soil and basalt layers) should be known at a small scale over the entire area of interest.

Lithologic characteristics are measured at only a sample of sites through evaluations of cores or geophysical logging of wellbores. Predictions of lithologic characteristics must be made between wellbore locations because hydrologic modelers seek to determine values over the whole area of interest, and they require information at many locations not sampled.

1.1 Purpose

The purpose of this report is to document prediction of these lithologic characteristics for the area in and around the SDA based on an updated evaluation of SDA lithology using lithologic information from wells drilled through 2003 (Ansley, Helm-Clark, and Magnuson 2004). The framework for the hydrologic model is the definition of the subsurface structure. At the SDA, the subsurface is a complex layering of basalt and sedimentary interbeds. The hydrologic model provides flow and transport predictions of contaminants of concern from known sources to the aquifer in support of the remedial investigation and feasibility study (RI/FS) for Waste Area Group (WAG) 7 Operable Unit (OU) 7-13/14 under the Comprehensive Environmental Response, Compensation, and Liability Act.[a]

1.2 Overview

Subsurface lithology was previously predicted using kriging models; however, since then, new wells have been drilled and errors in the database identified and corrected. Lithologic model predictions form the framework for hydrologic models used to predict fate and transport. Thus, the defensibility of the hydrologic predictions is based on the defensibility of the lithologic layer predictions. A simplistic depiction of the subsurface layers would produce unrealistic flow and transport predictions, and defensible predictions are necessary to make decisions regarding future actions at the SDA.

---

a. The *Federal Facility Agreement and Consent Order for the Idaho National Engineering Laboratory* (DOE-ID 1991) lists 10 WAGs for the INEEL. Each WAG is subdivided into OUs. The RWMC is identified as WAG 7 and originally contained 14 OUs. Operable Unit 7-13 (transuranic pits and trenches RI/FS) and OU 7-14 (WAG 7 comprehensive RI/FS) were ultimately combined into the OU 7-13/14 comprehensive RI/FS for WAG 7.

Treating spatially correlated values as independent values (i.e., using lithologic predictive models that do not incorporate spatial correlation) results in larger prediction uncertainty. Spatial correlation among values implies they are positively correlated with nearness; sample locations close to each other result in values that are more similar than sample locations far away. This relationship between similarity and distance is used to improve the accuracy and precision of predictions made at new locations in spatial modeling. The difference between various spatial models is how the spatial correlation is assumed or used.

1.3 Scope

This report describes the updated subsurface lithologic prediction process. The predictions are based on spatial models. Spatial models use the spatial correlation among sample values to improve predictions at unsampled locations.

The subsurface of the SDA can be described by the top elevation of each soil layer and its thickness. These values are obtained by interpreting information from wells. The current hydrologic model domain is from the surface down through the C-D sedimentary interbed. In the SDA, eight variables, detailed in Section 3, are predicted to form the framework for the hydrologic model. Each of the eight variables is predicted using a two-dimensional spatial model.

Appropriate spatial models are determined and predictions are calculated using data of lithologic characteristics. This report details the process of examining the relationship of measured lithologic variables to location variables, determining spatial correlation structure—including an investigation of anisotropy (directionally dependent spatial correlation)—calculating predictions, determining the fit of the spatial model, and examining spatial model uncertainty.

1.4 Document Organization

The following are brief descriptions of the remaining sections in this report:

- Section 2 provides a brief history and description of the SDA
- Section 3 describes the data used and their origin
- Section 4 describes the method used in this study, ordinary kriging, and method of spatial model assessment
- Section 5 presents the results for lithology variables, the predictions and standard errors, and results of spatial model assessment
- Section 6 discusses the value and meaning of the previous sections
- Section 7 lists the references cited throughout this report
- Appendix A contains directional variograms and an omni-directional variogram with model
- Appendix B contains graphs showing the kriging results and standard errors.

2. SITE BACKGROUND

The INEEL, originally established in 1949 as the National Reactor Testing Station, is a U.S. Department of Energy-managed facility that historically has been devoted to energy research and related activities. The name was changed to the Idaho National Engineering Laboratory in 1974 to reflect the broad scope of engineering activities taking place at various on-Site facilities. In 1997, the name was changed again to the Idaho National Engineering and Environmental Laboratory to be consistent with contemporary emphasis on environmental research.

The INEEL is located in Southeastern Idaho and occupies 2,305 km^2 (890 mi^2) in the northeastern region of the Snake River Plain. Regionally, the INEEL is nearest to the cities of Idaho Falls and Pocatello and to U.S. Interstate Highways I-15 and I-86. The INEEL Site extends nearly 63 km (39 mi) from north to south, is about 58 km (36 mi) wide in its broadest southern portion, and occupies parts of five Southeast Idaho counties. Public highways (i.e., U.S. 20 and 26 and Idaho 22, 28, and 33) within the INEEL boundary and the Experimental Breeder Reactor I, which is a national historic landmark, are accessible without restriction. Otherwise, access to the INEEL is controlled. Neighboring lands are used primarily for farming or grazing or are in the public domain (e.g., national forests and state-owned land). See Figure 1 for the location of the INEEL and major facilities.

2.1 Site Description

The RWMC, located in the southwestern quadrant of the INEEL, encompasses a total of 72 ha (177 acres) and is divided into three separate functional areas: the SDA, the Transuranic Storage Area, and the Administration and Operations Area. The original landfill, established in 1952, covered 5.2 ha (13 acres) and was used for shallow land disposal of solid radioactive waste. In 1958, the landfill was expanded to 35.6 ha (88 acres). Relocating the security fence in 1988 to outside the dike surrounding the landfill established the current size of the SDA as 39 ha (97 acres). The Transuranic Storage Area was added to RWMC in 1970. Located next to the east side of the SDA, the Transuranic Storage Area encompasses 23 ha (58 acres) and is used to store, prepare, and ship retrievable transuranic waste to the Waste Isolation Pilot Plant. The 9-ha (22-acre) Administration and Operations Area at RWMC includes administrative offices, maintenance buildings, equipment storage, and miscellaneous support facilities. See Figure 2 for a map of RWMC showing the location of the SDA.

The eastern Snake River Plain Aquifer underlies RWMC at an approximate depth of 177 m (580 ft) and generally flows from the northeast to the southwest. The aquifer is bounded on the northwest and southeast by the edge of the Snake River Plain, on the southwest by surface discharge into the Snake River near Twin Falls, Idaho, and on the northeast by the Yellowstone plateau. The aquifer is hosted in the fractured and layered basalt flows of the eastern Snake River Plain.

The regional subsurface mostly consists of layered basalt flows interbedded with comparatively thin sediments. Layers of sediment, referred to as interbeds, tend to retard infiltration to the aquifer and are important features in assessing the fate and transport of contaminants. In the 177-m (580-ft) interval from the surface to the aquifer, three major interbeds are of particular importance. Using nomenclature established by the United States Geological Survey, these sedimentary layers are referred to as the A-B, B-C, and C-D interbeds.

Lithologic characteristics of the subsurface are a key component in hydrologic modeling. Flow through subsurface media is variable, corresponding to the media itself. The subsurface at the SDA is a complex layering of basalt and soil interbeds. A simplistic pancake depiction of the subsurface layers would predict unrealistic fate and transport. Realistic predictions along with uncertainty provide the necessary framework for hydrologic models and contribute to more defensible decision-making.

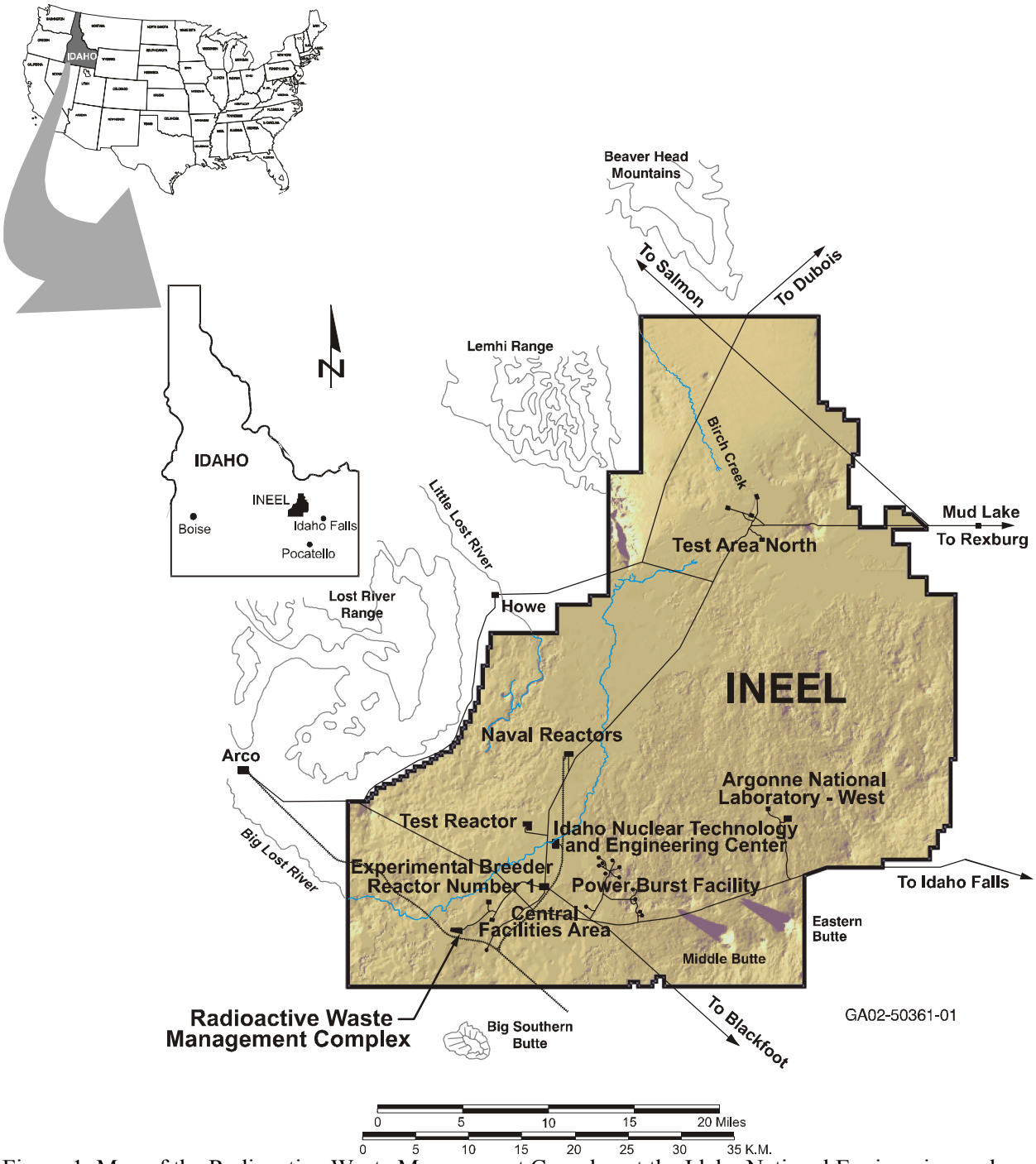

Figure 1. Map of the Radioactive Waste Management Complex at the Idaho National Engineering and Environmental Laboratory.

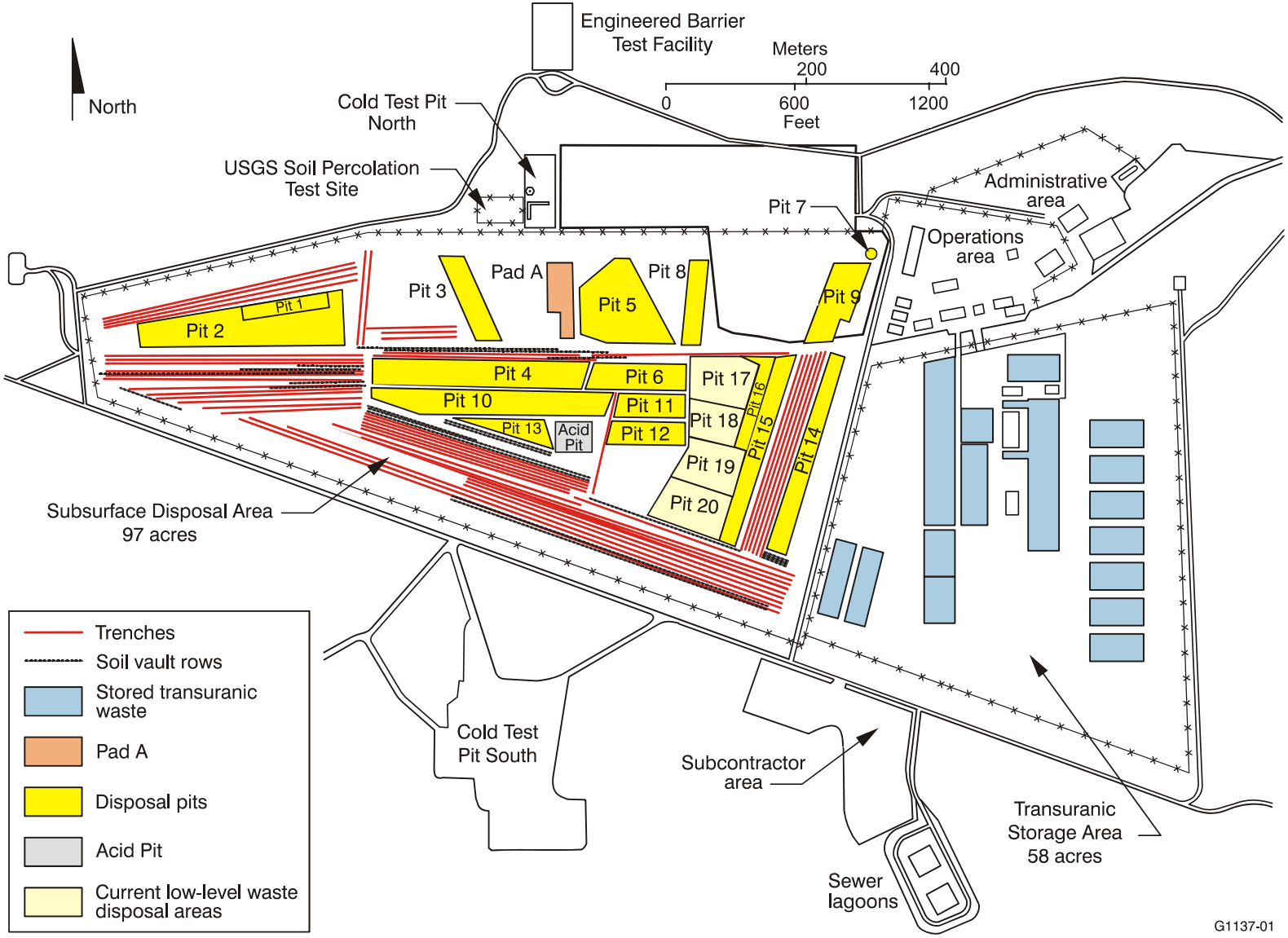

Figure 2. Map of the Subsurface Disposal Area at the Radioactive Waste Management Complex.

3. DATA

The geologic characteristics of the area are described in *Development, Calibration, and Predictive Results of a Simulator for Subsurface Pathway Fate and Transport of Aqueous- and Gaseous-Phase Contaminants in the Subsurface Disposal Area at the Idaho National Engineering and Environmental Laboratory* (Magnuson and Sondrup 1998). The data used here are based on *Updated Stratigraphic Selections for Wells in the Vicinity of the Subsurface Disposal Area* (Ansley, Helm-Clark, and Magnuson 2004) with interpretations for basalt and sediment interfaces derived from data on wells drilled through 2003.

The lithology data set (Ansley, Helm-Clark, and Magnuson 2004, Appendix B) was used to predict lithology layers on four prediction grids over the area of interest (see Figure 3). Sample site locations were reported in state plane coordinates in the North American Datum of 1927 (i.e., NAD 27), which is historically used on the INEEL (see Figure 4). This lithology data set consisted of 133 sample sites where bore holes were drilled and elevation measurements taken at the top elevation and thickness of the interbed soil layers. Eighteen layers were measured, but only eight were used in the analyses documented in this report. These layers are listed below:

- Surface elevation
- Surficial soil thickness
- Elevation of the top of the A-B interbed soil layer
- Thickness of the A-B interbed soil layer
- Elevation of the top of the B-C interbed soil layer
- Thickness of the B-C interbed soil layer
- Elevation of the top of the C-D interbed soil layer
- Thickness of the C-D interbed soil layer.

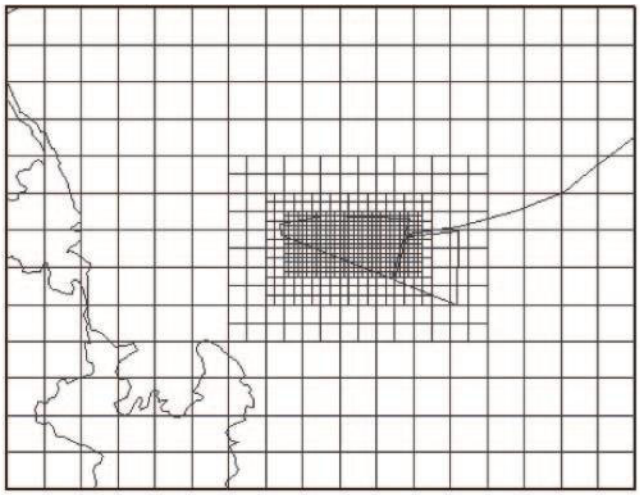

Figure 3. Prediction grids over the area of interest for the Subsurface Disposal Area.

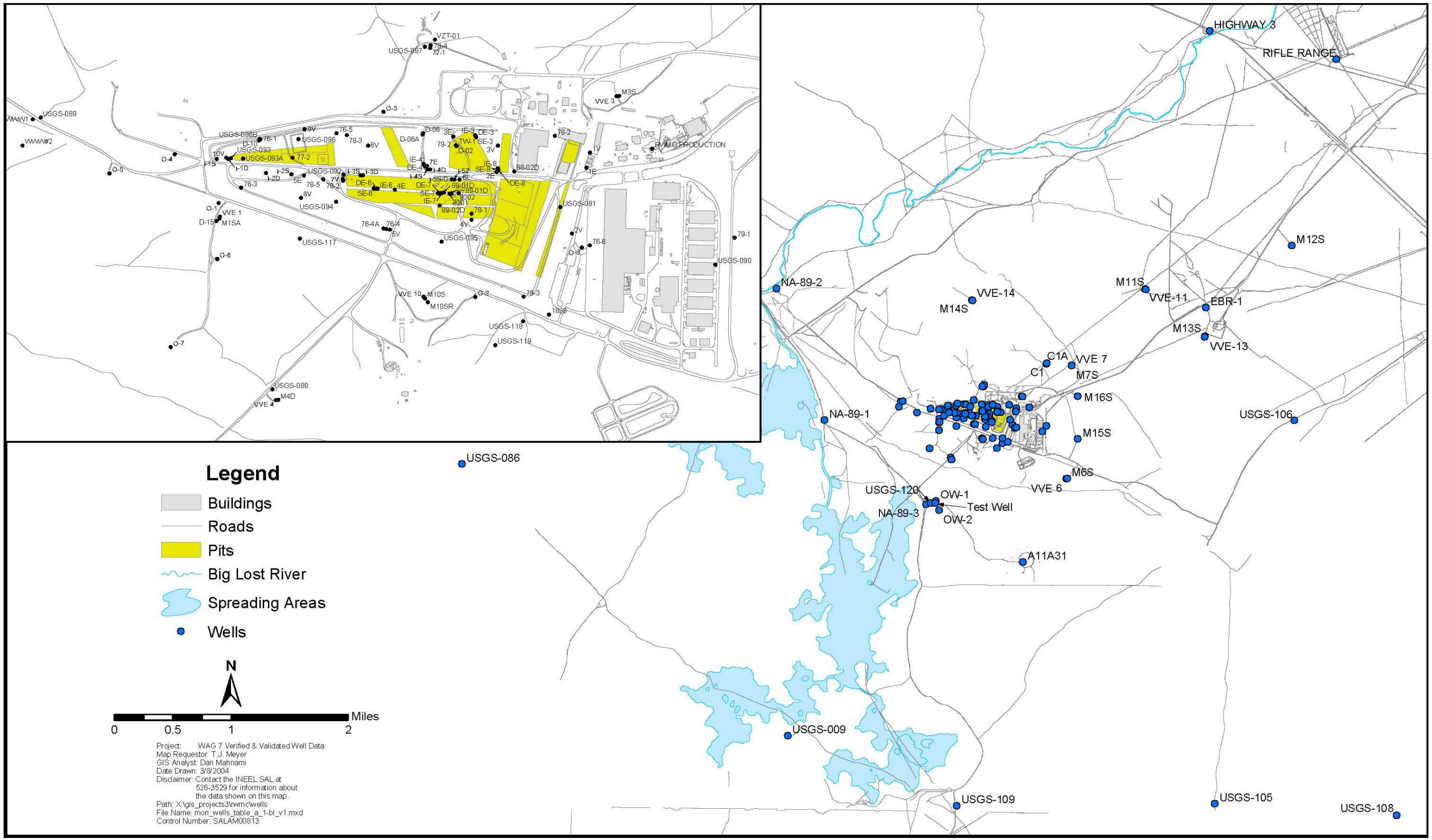

Figure 4. Location of wells deeper than the surficial sediment that were used to obtain lithology information.

Because there are a greater number of shallow wells drilled than deeper wells, there is more information on lithologic characteristics in the shallower interbed layers. As a result, the distance between information sites in the lower layers (i.e., D basalt layer and D-E interbed soil layer) exceeded the spatial correlation range of the data. The D basalt layer, D-E interbed soil layer, and any deeper layers had too few sampled sites to consider spatial modeling.

In 44 instances, an interbed layer was drilled into but not through. Thus, the measured thickness for the interbed is reported as greater than the thickness at the deepest point in the hole. This occurred once in the A-B interbed, seven times in the B-C interbed, and 36 times in the C-D interbed. Leecaster (2002) estimated thickness from a regression on the upper layer elevation and thickness values. Although the relationships were statistically significant, the resulting kriging predictions were almost identical to those using the truncated values. The estimated values exaggerated the thickness of the interbeds, so they were not used in previous spatial modeling. Therefore, an estimation procedure also will not be used in this spatial modeling effort.

The region covered by the 133 wells is oval-shaped with major axis in the northeast to southwest direction, following the general direction of flow of the Snake River Plain Aquifer. The distance among pairs of sample locations ranges from 2 to 6,892.4 m (6.7 to 22,613 ft); most of them are less than 1,524 m (5,000 ft). The direction-specific pairwise distances in the north-south and southeast-northwest directions are mostly less than 762 m (2,500 ft) (see Figure 5). Thus, anisotropy could be assessed through directional variograms only within about 762 m (2,500 ft) to ensure at least 50 sample pairs for each distance lag.

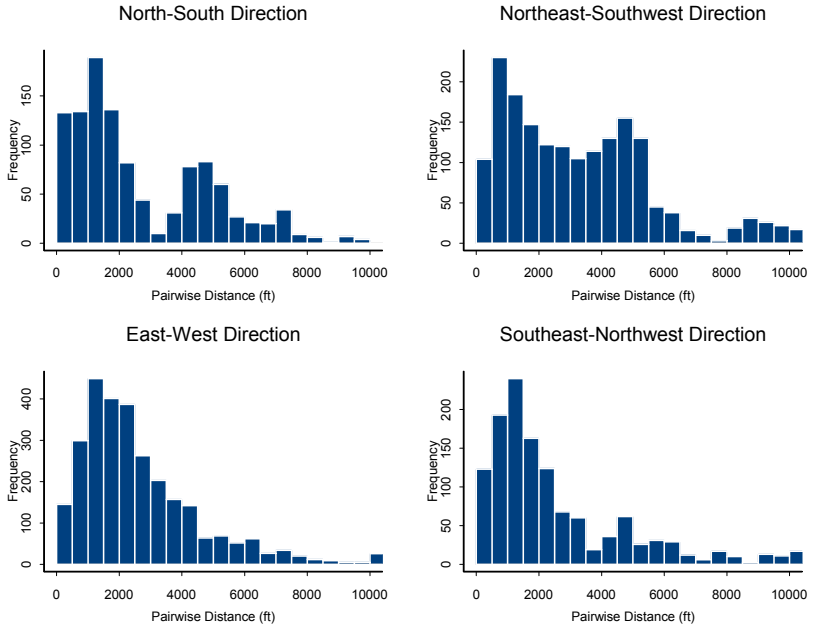

Figure 5. Pairwise distances among 133 well locations in four directions, within 22.5-degree tolerance.

The surface elevation was obtained from an INEEL flyover (Aero-Graphics 2000). This 61-m (200-ft) aerial photogrammetric imagery was processed into planimetric and 0.6-m (2-ft) contour data. There were elevations provided on a 3-m (10-ft) grid, resulting in 972,000 locations. The data extended beyond the RWMC but not to the full extent of the area of interest.

Despite the great amount of data, the surface elevation was modeled on the prediction grid for two reasons: (1) predicted elevations were required for the whole area of interest and the flyover data did not extend that far, and (2) the data set was too large to use as input into the hydrologic model. A random sample of 1,000 locations from the flyover was combined with the elevation of the ground surface at well locations to predict surface elevation on the prediction grids (defined in the methods).

4. METHODS

The data were assessed for distribution and extreme values. The measured values were then assessed for spatial correlation using variograms. These variograms were used to calculate kriging predictions and standard errors. Finally, the spatial model was assessed for fit to the data.

Spatial model predictions are generally made on a regular grid. This grid definition is based on how the predictions will be used as well as on the spatial continuity of the variable. For the SDA, predictions are made for four prediction grids. These grids are rectangular and of decreasing size and increasing intensity based on the hydrologic model discretization (see Figure 3 and Table 1). The largest grid will be called Grid 0, the next smallest will be called Grid 1, then Grid 2, and the smallest will be called Grid 3. The four grids were devised to cover a large region with a coarse grid and successively smaller areas with finer grids, which are of greater interest for the hydrologic model. The grid cells range in size from 38.1 to 304.8 m^2 (125 to 1,000 ft^2). The results from the grids were then combined so that smaller-area grid (i.e., interior) predictions had precedence over larger-area grid predictions. This map of the whole area with different grid intensities in different areas was used as input for the hydrologic model.

Table 1. Prediction grid descriptions.

	Grid 0	Grid 1	Grid 2	Grid 3
Easting cell size	1,000 ft	500 ft	250 ft	125 ft
Number of cells	17	14	18	28
Total length	17,000 ft	7,000 ft	4,500 ft	3,500 ft
Northing cell size	1,000 ft	500 ft	250 ft	125 ft
Number of cells	13	10	12	14
Total length	13,000 ft	5,000 ft	3,000 ft	1,750 ft

The data were reported as elevation at the top elevation and thickness of interbed soil layers. These fully define the layer structure. Various structure definitions were explored in *Geostatistic Modeling in the RWMC Region* (Leecaster 2002) and were found to produce equivalent results. There and here, predictions were reported as elevation at the top of and the thickness of the soil layer (surficial or interbed).

4.1 Data Assessment

For each lithologic layer variable—elevation and thickness—the data were assessed for symmetry. Kriging does not assume normality but relies on symmetry of distribution. This was assessed by Shaprio-Wilk tests and visually from histograms and normal probability quantile-quantile plots.

Any extreme values (large thickness and large or small elevation), which might represent local nonstationarity, were identified using histograms or stem-and-leaf plots. Extreme values would not be removed, but their effect on variograms and kriging predictions would be investigated.

4.2 Variograms

The empirical variogram for a set of data is the corresponding values of distance and variance between pairs of values at that approximate distance. The empirical variogram is then fit with a model, and those model parameters are used to calculate kriging predictions.

The empirical variogram for a set of data depends on at least three input values. These input values specify the maximum distance for the variogram and the distance lag and lag tolerance between pairs of locations that are combined to provide one point on the variogram. For nonsystematic sample locations, the distance between pairs of points is not regular, so pairs of points at an approximate distance are combined to provide one point on the empirical variogram. Thus, the distance lag must be specified as well as the tolerance around that lag (plus or minus some distance from the target lag).

The maximum distance for the variogram is generally recommended to be no more than one-half the maximum distance among sample locations. For most applications, maximum distance among sample locations is the same as the maximum distance of the prediction grid, because extrapolation is rarely beneficial. In the present application, some of the four prediction grids are much smaller than the maximum distance among sample locations. Thus, for this work, the maximum distance for the empirical variogram will reflect the maximum prediction grid instead of the data locations. Therefore, for each lithologic variable, there will be four unique values for the maximum distance, corresponding to the four prediction grids. The maximum distance of the variogram for each of the four different empirical variograms was set to be approximately one-half the size of the prediction grid corresponding to that variogram. The maximum distance for the variogram (see Table 2) used was approximately one-half the average of the easting coordinate distance and the northing coordinate distance because the prediction grids were not square.

Table 2. Input parameters for empirical variograms and kriging predictions for four prediction grids.

Grid	Maximum Distance (ft)	Lag Distance (ft)	Lag Tolerance (ft)	Search Radius (ft)
0	8,000	500	250	7,000
1	3,000	250	125	2,500
2	2,000	125	65	1,200
3	1,000	65	33	900

The distance lag and lag tolerance should be specified to provide at least 30 pairs of sample locations for each point on the empirical variogram. At least 30 pairs are necessary to produce a reliable estimate of the variance. If the data are put into too many distance lags with few pairs in each, then the empirical variogram is generally sporadic and difficult to model. If the data are lumped into too few distance lags, then spatial correlation is difficult to determine. The distance lag and lag tolerance should be specified to provide enough detail in the empirical variogram at the range appropriate to the prediction grid to allow it to be modeled.

The prediction grids were used as a guide to the distance lag and were calculated in four different empirical variograms for each layer. For the smallest interior grid, the grid cells are 38.1 m^2 (125 ft^2), so the lag is specified to be approximately one-half that, 19.8 m (65 ft), to ensure 30 pairs of locations for each empirical variogram point. For the next largest grid, the grid cells are 76.2 m^2 (250 ft^2), so 38.1 m (125 ft) is the specified lag. The lags are specified similarly for the other two grids (see Table 2). The lag tolerances were set to be one-half the distance lag. This is generally recommended because it allows for the most pairs to be included in a distance lag without allowing pairs to overlap into two distance lag classes.

The empirical variogram can be calculated using at least two methods: classical and robust. The classical variogram is estimated as one-half the squared difference between values at lag (plus or minus tolerance) distance divided by the number of pairs within a lag class (lag class is the lag plus or minus

tolerance) (Matheron 1963). The robust estimator (Cressie and Hawkins 1980) of the variogram uses the square root of the absolute difference between pairs of values divided by the number of pairs, raised to the fourth power, and divided by a constant to correct for bias. The robust estimator provides stability in estimates for skewed data or data with outliers. The classical variogram estimator was used for elevations (which are generally symmetric) and robust variogram estimators for thickness values (which are generally skewed although not log-normal).

Directional variograms also were computed to investigate anisotropy. Anisotropy is the dependence of spatial correlation on direction. The directional variograms were compared for four directions corresponding to north-south (0 degrees), northeast-southwest (45 degrees), east-west (90 degrees), and northwest-southeast (135 degrees). The directional variogram was calculated using only pairs that were in the specified direction, plus or minus a tolerance angle of 22.5 degrees. Data that display similar variograms for all directions are considered isotropic.

The input parameters to the kriging equations come from a model for the empirical variogram. There are various methods to automatically fit a model to the variogram, but fitting the variogram by eye is generally preferable. The variogram model is a function of the:

- Model: many are possible; Gaussian or spherical was used
- Nugget: small-scale variation
- Sill: asymptotic variance between independent pairs of sites
- Range: distance at which the sill is attained.

The model is chosen based on the shape of the empirical variogram. A Gaussian model has a very slight slope and curves up like a stretched-out S (see Appendix A, Figure A-11, Grid 0). This model has been used for spatially continuous variables, such as land surface or aquifer elevation. The spherical model has an immediate steep slope that tapers off (see Appendix A, Figure A-11, Grid 3). This is a popular model and does not assume a strong nearby spatial correlation, unlike the Gaussian model.

The nugget is the small-scale or measurement variation. If the sample locations are close enough, then this is easily estimable. A zero nugget is reasonable and indicates small measurement error. Specifying a zero nugget, even without ample close-range data, is appropriate if the variance of the data (sill) is large.

The sill is the variance of pairs of locations assumed to be independent. This value can be larger or smaller than the variance of the data overall, depending on the sample locations. The sample variance of many close locations will provide an underestimate of the sill, while the sample variance of many far-flung locations may overestimate the sill. The partial sill is used in kriging equations and is reported here. The partial sill is the asymptotic variance (sill) minus the nugget. The partial sill is sometimes called the contribution for a model structure.

The range is the distance at which sample locations are independent. This is termed an effective range for the Gaussian model because the slope at the sill is slightly greater than zero.

An empirical variogram may be modeled by a combination of model structures. There may be more than one level of spatial correlation, corresponding to nested structures. The variogram model parameters are used in the kriging equations, so they should correspond to the prediction grid. For this reason, a variogram for each grid was separately calculated and modeled. So although the variogram

overall may have contained multiple structures, when calculated using the appropriate lag distance and maximum distance, one-structure variograms emerged.

4.3 Ordinary Kriging

Ordinary kriging was used to predict lithologic layers over the area of interest. Kriging produces best linear unbiased predictions and takes into account the spatial relationship among sample values. The kriging predictions are based on a weighted mean of all sample values. The weights depend on variogram parameters discussed above. Unlike spatial conditional simulation, kriging produces one representative realization. Spatial conditional simulation generates a large set of realizations.

The two assumptions for kriging are (1) location invariant spatial correlation (i.e., stationarity) and (2) isotropy (i.e., spatial correlation is independent of direction). Local stationarity is assumed for ordinary kriging. This is reasonable for the elevation and thickness values because the spatial correlation is not expected to change over the prediction area. Isotropy must be verified through investigation of directional variograms. Two assumptions are specific to ordinary kriging (not assumed for other types of kriging). The first is a local, unknown mean. The second is the coefficients sum to one, which ensures uniform unbiasedness in the predictions.

Block ordinary kriging was used to calculate the predicted elevation and thickness values. Block kriging assigns the mean prediction over a block area. Predictions are calculated on four grids as defined for the hydrologic model. The grid cell size varies from 38.1 m^2 (125 ft^2) to 304.8 m^2 (1,000 ft^2). The average prediction over the grid cell (the result of block kriging) is more realistic than the prediction at the center point of the grid cell (the result of point kriging) and also results in less kriging model uncertainty.

The kriging algorithm requires input parameters to specify the block dimensions, the minimum and maximum number of data points to use in each calculation, and the search radius for data points to use in the prediction. These input parameters are interconnected and depend on the others' definition. The block dimensions define the area to be averaged to determine the prediction for a grid cell. These will match exactly the four prediction grids. Theoretically, kriging is a global predictor, meaning all data points are used to make predictions at each point. In practice, a few sample points are used to calculate predictions in order to avoid oversmoothing of the surface and to improve calculation efficiency. The number of sample points to use depends on the density of the data and the smoothness desired. These data are patchy; many sample locations are in the SDA, and a few are outside of that area. Oversmoothing is not conservative for groundwater risk modeling, so a rougher surface is desired. Up to five sample points to calculate each prediction are used. Note that the weights from the variogram are used on these five points so that closer locations have greater influence. The minimum number of data points to use in prediction is specified along with the search radius. This is to ensure that prediction grid cells far removed from the data locations have this minimum number in the calculation. The minimum number of sample values to use in prediction is one because there were areas far-removed from sample data that should not be influenced by even farther-removed data. The search radius limits these five points from being too far away from the prediction location to be useful (see Table 3). These values were specified to ensure that every grid cell could be predicted (at least one sample value was within that distance) and that the predictions were not influenced by far-reaching sample values.

Ordinary kriging and cross validation (discussed below) were performed in *GSLIB: Geostatistical Software Library and User's Guide* (Deutsch and Journel 2000), and variograms were calculated and fitted in S-PLUS Spatial Module (S+SPATIALSTATS).

Table 3. Variogram model parameters for all grids.

Lithologic Layers	Grid 0 (Various Models)				Grid 1 (Spherical Model)			Grid 2 (Spherical Model)			Grid 3 (Spherical Model)		
	Model	Nugget (ft^2)	Partial Sill (ft^2)	Range (ft)	Nugget (ft^2)	Partial Sill (ft^2)	Range (ft)	Nugget (ft^2)	Partial Sill (ft^2)	Range (ft)	Nugget (ft^2)	Partial Sill (ft^2)	Range (ft)
Surface Elevation	Spherical	0	375	6,200	0	375	6,200	0	375	6,200	0	375	6,200
Alluvium Thickness	Gaussian	3	37	1,000	3	37	400	3	37	400	3	37	400
Top A-B Interbed Elevation	Gaussian	30	900	5,000	30	140	2,500	30	140	2,500	10	60	400
A-B Interbed Thickness	Spherical	2	6	750	2	6	750	2	6	750	2	6	400
Top B-C Interbed Elevation	Gaussian	7	180	6,000	5	25	2,500	4	18	1,000	3	13	500
B-C Interbed Thickness	Spherical	8	210	7,000	8	90	2,500	8	50	1,200	8	25	600
Top C-D Interbed Elevation	Gaussian	10	120	3,000	7	30	2,500	7	20	1,500	3	13	500
C-D Interbed Thickness	Spherical	40	70	1,000	40	70	1,000	40	70	1,000	40	60	400

4.4 Model Assessment

Cross validation was performed for the kriging predictions in order to assess the fit of the kriging model. Hold-one-out point predictions were made for each sample location without using that sample as part of the prediction. Point instead of block kriging was used to compare points to points, instead of cell means to points. Each site had an associated hold-one-out error equal to the hold-one-out prediction minus the measured value. Large errors indicate inadequacies of the kriging model or large influence of the site value. A site value has large influence if it is extreme with respect to nearby values, or if, far from other sites, it is extreme with respect to other values.

The variogram model used to produce the hold-one-out kriging predictions corresponded to those specified in Table 3. Because the sample size was large, removing one value did not affect the variogram, so variograms from all sample values were used. Separate analyses of the cross-validation results were performed for each prediction grid and included only those sample locations within the boundaries of that prediction grid.

The cross-validation results were summarized by mean error, median of the errors, as percent of measured value, mean square error (MSE), and square root of the reduced MSE. The reduced MSE is mean of the square of each error divided by its kriging variance. The square root of the reduced MSE is near unity and within the limits of $1 \pm 2\sqrt{2/n}$ for a model that fits well (Magnuson and Sondrup 1998).

The cross-validation results also were investigated visually using graphs. The measured values were plotted against the cross-validation predicted values to help assess the accuracy of the predictions. The histograms of cross-validation errors were used to assess kriging model adequacy by looking for outliers, skewness, and multimodality. Histograms of measured values and cross-validation predictions were compared for relative frequency of values and range of values.

All plots and summary statistics were computed, but only those grids used for hydrologic modeling for specific lithologic layers are included in this report. Surface and A-B layers were restricted to locations within the Grid 3 boundary. The B-C layers were restricted to locations within the Grid 2 boundary. The C-D layers were considered for locations within the Grid 1 and 0 boundaries, separately.

Plots of kriging predictions were overlain with sample values to demonstrate the correspondence between measured and predicted values. These are presented as part of the kriging prediction results, not with the other kriging model assessment results.

5. RESULTS

The data will be presented through exploratory means first. Next, the variograms and anisotropy results will be presented for all lithology variables. This will be followed by presentation of the predictions and standard errors. Finally, the kriging model assessment will be presented.

5.1 Exploratory Data Analysis

The data values for the lithologic variables were explored for distribution, extreme values, and correlations. Kriging assumes that data are symmetric but not necessarily normally distributed. This assumption is investigated through histograms and stem-and-leaf plots.

The elevation variables are generally symmetric with no extreme values, although some have long tails (see Figure 6). The thickness variables are generally skewed right (see Figure 6). The values, however, do not follow a log-normal distribution. No transformation was used on the thickness values, but robust variogram estimates were used to allow for nonsymmetry.

5.2 Variograms

Four variograms were calculated for each lithologic layer variable based on the four prediction grids. The maximum distances and lag distances are provided in Table 2. The resulting variogram parameters (discussed below) are provided in Table 3. The four empirical variograms for a single lithologic variable were sometimes different. One explanation is that the true spatial variance had more than one structure, so it would appear steplike over the entire range. This can be modeled as a multistructure variogram or as separate variograms, as was done here. Empirical variograms for some lithologic variables on Grid 0 appear to be poorly fit by the variogram model. Grid 0 empirical variograms use a large lag distance that is sometimes greater than the spatial range of the data but is determined by empirical variograms on smaller prediction grids that use smaller lag distance. Anisotropy was discounted for all elevation and thickness variables. In some cases, discussed separately below, there was suggestion of anisotropy. The possible anisotropy was generally limited by the sample locations. There were limited data in the north-south and southeast-northwest directions, especially beyond 762 m (2,500 ft) (see Figure 5). Thus, even though anisotropy could be investigated in two directions, the directions were not perpendicular. Also, the anisotropy for Grid 3 could have been incorporated but was never predominant enough to include in the variogram model. Goovaerts (1997) recommends, “An anisotropy that is not clearly apparent on experimental variograms nor backed by any qualitative information is better ignored.” Based on this advice and investigation of the directional variograms, isotropic models were fit to all lithologic layer variables.

The reported variogram parameters are the model, nugget, partial sill, and range. The model is either Gaussian or spherical. The nugget is in squared feet (as a variance). The partial sill is the sill minus the nugget in units of squared feet. The range is reported in feet.

The variograms for the surface elevation differed from other lithology layers. The large set (n = 1,133) of values resulted in a very precise variogram with the same structure for all four prediction grids (see Appendix A, Figure A-9). Thus, one variogram was used for all four grids (see Table 3). The spherical model fit this large data set, although elevations generally are modeled with a Gaussian model. Anisotropy for the surface elevation was discounted based on four directional variograms (see Appendix A, Figure A-1). The setup for Grid 0 is considered because of the large range and absence of different structures for the other grids. Although the directional variograms deviate from the model between 61 and 2,133.6 m (200 and 7,000 ft), they reach the same final sill and approximate range. The hump in the north-south and southeast-northwest directions at about 5,000 ft is because of a group of sample locations at that distance (see Appendix A, Figure A-1), whereas there are few pairs at closer and farther distances.

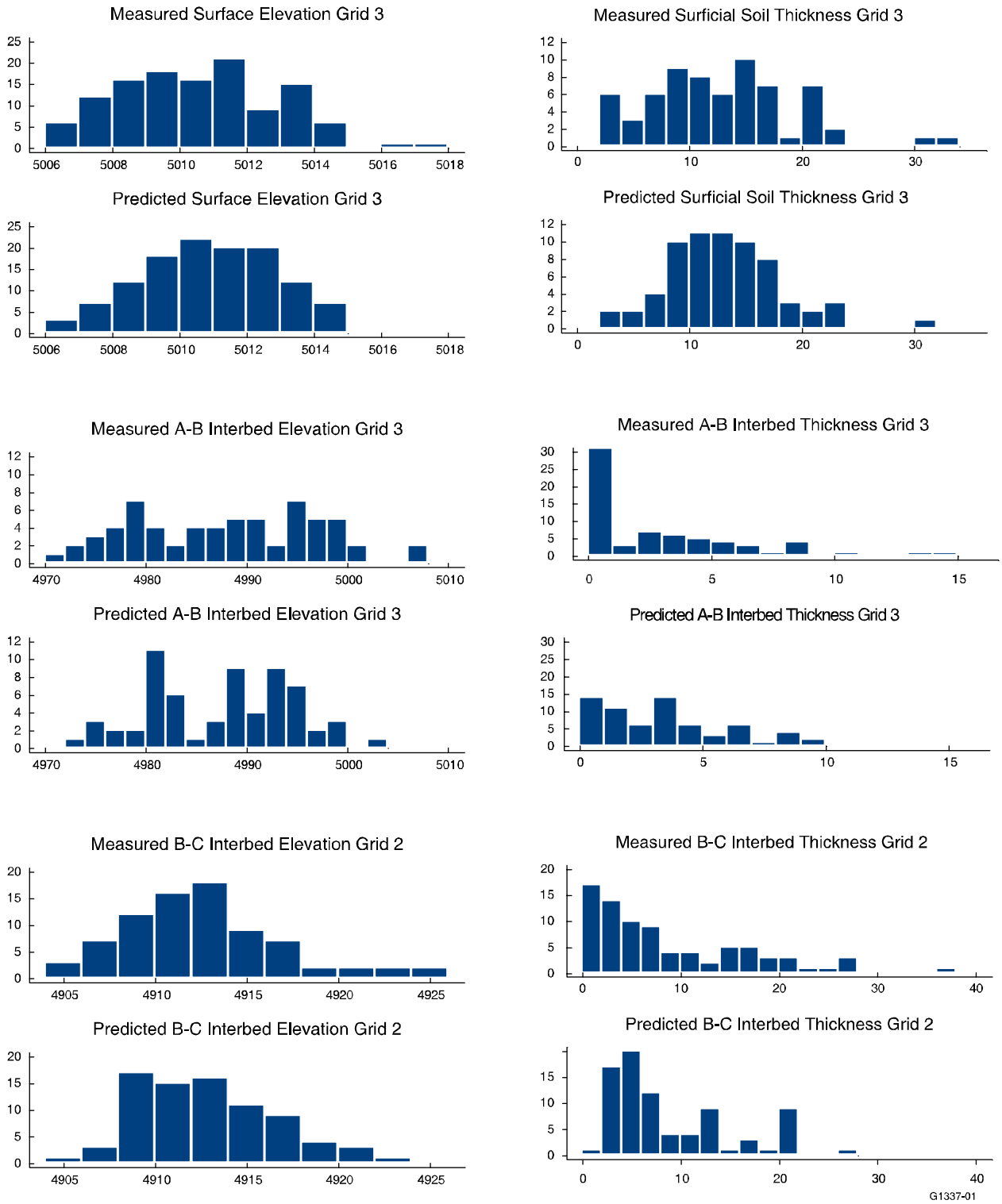

Figure 6. Histograms of measured and predicted lithologic variables for layers and grids to be used in the hydrologic model.

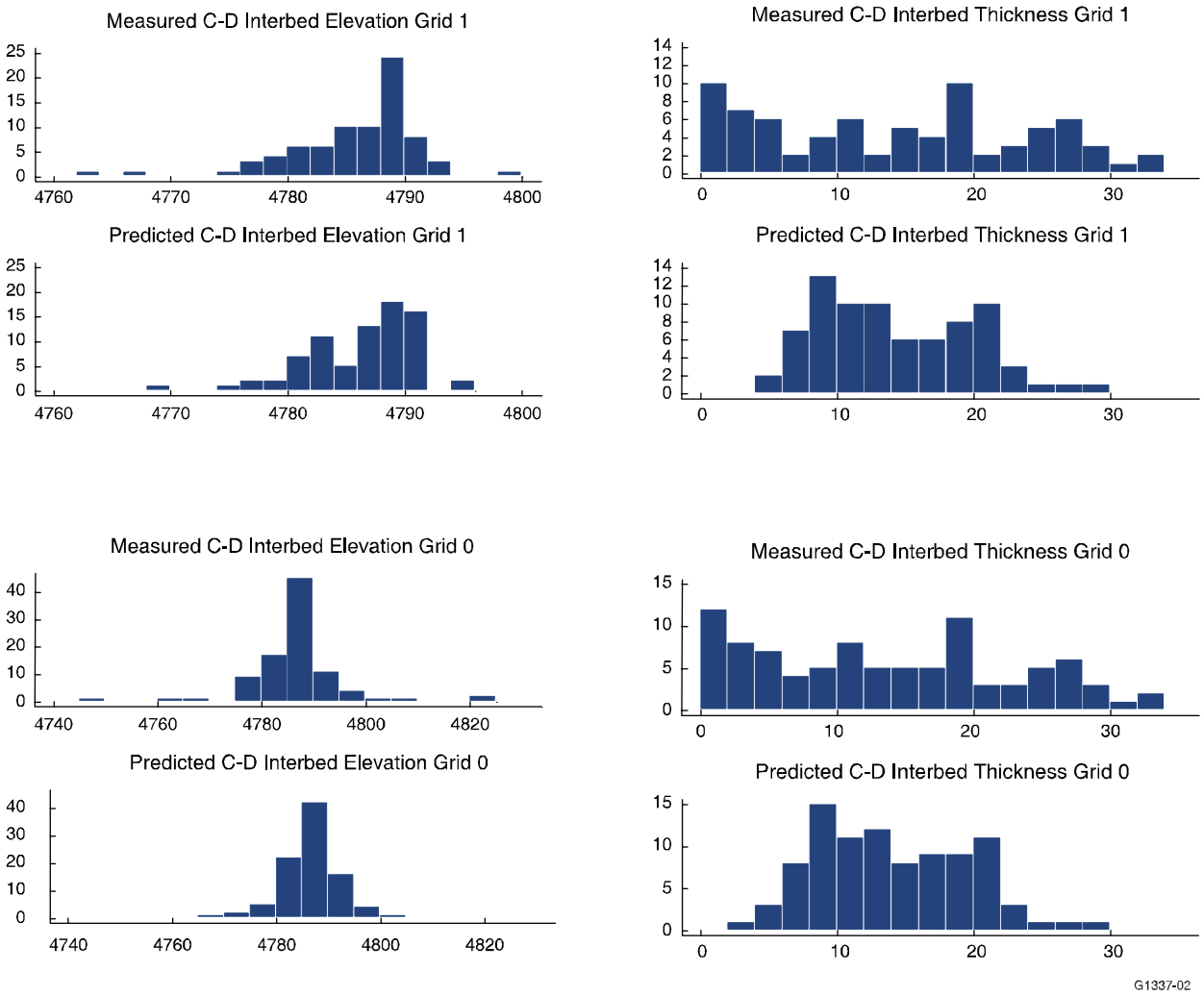

Figure 6. (continued).

The surficial soil thickness variograms were also similar for all four grids (see Appendix A, Figure A-10). Despite this, a Gaussian model was used for the Grid 0 variogram in order to provide kriging predictions that reflected the observed values and did not predict the overall average thickness for the outlying areas. Spherical models were used for the other grids because they fit the shape of the empirical variogram better (see Table 3). Anisotropy was discounted based on the four directional variograms (see Appendix A, Figure A-2).

The elevation at the top of the A-B interbed variograms differed somewhat by prediction grid (see Appendix A, Figure A-11; Table 3). The Grid 1 and 2 variograms were modeled the same, although the range for Grid 2 was beyond the maximum distance for Grid 1. This was done to preserve the spatial correlation structure seen overall, not artificially restricted to the maximum distance for the prediction grid. The Grid 0 variogram was fit with a Gaussian model, while the other variograms were fit with spherical models. The Gaussian model on the largest grid allows expression of the data values without being overwhelmed by the smoothing process over such large blocks. Isotropy was assumed based on the four directional variograms (see Appendix A, Figure A-3). For Grids 1 and 2, the north-south direction displayed slightly higher sill. This may be the overriding influence on Grid 0, which has a larger sill, and as seen from the directional variograms for Grid 0, the other directions have lower sill. These differences

seem slight, and the problem with modeling the anisotropy is that there are limited location pairs in the north-south direction past 609.6 m (2,000 ft).

The A-B interbed thickness required only two variograms for the four grids. Only the smallest grid, Grid 3, displayed a shorter range than the rest (see Table 3; Appendix A, Figure A-12), although the nuggets and partial sills were the same. Isotropy was assumed based on the four directional variograms (see Appendix A, Figure A-4).

The elevation at the top of the B-C interbed required four different variograms for the four prediction grids (see Appendix A, Figure A-13; Table 3). The large grid was modeled with a Gaussian model, and the other grids were modeled with a spherical model. Isotropy was assumed based on the four directional variograms (see Appendix A, Figure A-5). The sill for the northeast-southwest direction is slightly less than that for the southeast-northwest direction. Again, the difference is small, and the limited number of pairs past 609.6 m (2,000 ft) in the southeast-northwest direction hinders modeling any perceived anisotropy.

The B-C interbed thickness variograms were fit with four different spherical models (see Appendix A, Figure A-14; Table 3). Isotropy was assumed based on the four directional variograms (see Appendix A, Figure A-6).

The elevation of the C-D interbed required four different variograms for the four prediction grids (see Appendix A, Figure A-15; Table 3). The large grid was modeled with a Gaussian model, and the other grids were modeled with a spherical model. Isotropy was assumed based on the four directional variograms (see Appendix A, Figure A-7). The southeast-northwest variogram has a slightly larger sill, but not significantly so, and is especially past a lag of 609.6 m (2,000 ft), where fewer location pairs exist.

The C-D interbed thickness required only two variograms, both spherical (see Appendix A, Figure A-16; Table 3). The smallest grid displayed a smaller range and sill than the other grids. Isotropy was assumed based on the four directional variograms (see Appendix A, Figure A-8).

5.3 Kriging Predictions and Standard Errors

Contour plots of the block ordinary kriging predictions and standard errors are included for a subset of the grids, varying by layer (see Appendix B). The surface elevation, and A-B elevation and thickness are presented for Grid 3 only; B-C elevation and thickness for Grid 2 only; and the C-D elevation and thickness for Grids 0 and 1. Current hydrologic modeling for the vadose zone for OU 7-13/14 uses only Grids 1, 2, and 3. Grid 0 is included as it may be used in the future in evaluations of spreading area influences in the vadose zone.

The thickness plots contain areas that are predicted to be 0 ft. This reflects the data. Areas where one zero thickness is surrounded by nonzero thickness data are not necessarily predicted to be zero thickness, owing to the noninterpolative (may not reproduce data values) nature of kriging. Despite this, the predictions are generally very close to the sample values as described in Section 4.4.

There are cases of overlapping predictions. Overlap occurred when the predicted elevation of one layer was greater than the predicted elevation of the layer above it. Alternating kriging models for elevation and thickness minimized this error. Almost all of these overlaps occurred on grids and in layers that were not included in the hydrologic model. There were 44 prediction overlaps on Grid 3 for the surface elevation and the A-B interbed elevation, which are included in the hydrologic model. These predictions would imply that both the surficial soil and A-basalt layers had zero thickness. There are no data to support zero thickness in the surficial soil, and no zero thickness values were predicted on any of

the grids. In practice, the A-B interbed elevation was set to the surface elevation minus the surficial soil thickness. Thus, the predictions include zero thickness for the A-basalt layer, which occurs frequently in the sample data, so they are not unrealistic. The overlaps are caused by random variation and are not large, all less than 1.8 m (6 ft). There were also overlaps in grids and layers that were not included in the hydrologic model. These were dealt with in similar fashion but are not discussed specifically.

The kriging standard error is a function of the variogram model and the sample locations. The standard error is smaller near sample locations and larger away from sample locations. The kriging standard errors have similar patterns as a result of sample location with the exception of the surface elevation (see Appendix B, Figure B-3). The surface elevation kriging standard errors are based on 1,133 sample locations instead of the at most 133 well locations used for each lithologic variable. This accounts for the small kriging standard error, despite the large sill of 375. The magnitude of the standard errors is a function of the nugget and partial sill in the variogram model. If the partial sill is small, then the range of standard error values is small because the nugget and asymptote of the variance are approximately the same. If the partial sill is large, then large ranges of standard deviation are seen. The kriging standard errors for C-D interbed elevation are large (2–12 degrees) because of the large partial sill (120) (see Appendix B, Figure B-15). For the various grids, the standard errors and their ranges should vary. Larger grids should have larger and greater ranging standard errors because there are areas with dense sampling and areas with almost no samples. The small grids have good coverage overall, so standard errors should stay smaller. With the exception of the A-B interbed elevation (see Appendix B, Figure B-7), which has a partial sill of 60, the standard errors are small for the Grid 3 predictions. The kriging standard errors get progressively larger with increasing grid size.

5.4 Model Assessment

The cross-validation statistics indicate good-fitting kriging models (see Table 4; negative error statistics indicate underprediction). The mean error values are all very small, as expected from discussion of the results. The only large error as percent of truth is for the A-B interbed thickness on Grid 3, which is because of several thick interbed locations being predicted as small thickness, even zero (see Appendix B, Figure B-6). This occurred in places where large and small thickness values were close together. Although the MSE values seem large for most layers, the square root of the reduced MSE values, which put the MSE in relation to the kriging variance, is near one for all layers. This measure exceeds the ad hoc limit for the A-B interbed thickness on Grid 3 and the B-C interbed thickness on Grid 2. The reason for these large statistics may be the mixture of zero and large thickness values at nearby locations. This would be difficult for any model to predict accurately.

The distribution of the hold-one-out errors was generally symmetric and unimodal (see Figure 7). There were a few extreme values, either high or low, but not an unexpected number from the large number (up to 133) of data locations.

The errors for the C-D interbed thickness for Grids 1 and 0 have light tails and are moderately large. The heavy tails of the C-D interbed thickness error distributions may indicate inadequacy in the kriging model. Errors are expected to be small and clustered around 0; these are evenly spread between –10 and 10. This indicates inadequacy because errors are uniform indicating a kriging model that predicts the mean of the data without much variability to follow the data values. Fewer data locations are at this depth, and spatial correlation is not as strong (see Appendix A, Figure A-16 and Appendix B, Figure B-14).

The plots of measured versus predicted, from a hold-one-out approach, provide an assessment of the accuracy of the predictions (see Figure 8; the solid line is the one-to-one line and dotted lines are plus and minus two kriging standard errors). For the most part, predictions are within two kriging standard

deviations of the measured values. There are several measured zero thickness values in the A-B interbed that are not predicted to be zero. Those that are missed are generally near nonzero thickness values (see Appendix B, Figure B-6). The C-D thickness predictions are not, in general, related to the measured thickness, although most predictions are within two kriging standard errors (see Figure 8). The reason for the apparent independence of the predictions and the data that were used to produce them is the variogram. The variogram displays a large nugget, especially compared to the sill (see Table 3 and Appendix A, Figure A-16). This relatively flat variogram produces approximately equal weights for all data values used in prediction. The resulting predictions are not surprising given the large amount of variability in nearby location values.

Table 4. Cross-validation statistics for lithology data variables and layers used in hydrologic model.

Lithology Layer	Grid	Mean Error (ft)	Median Error as Percent of Truth (%)	Mean Square Error (ft^2)	Square Root of Reduced Mean Square Error (ft)
Surface elevation	Grid 3	-0.01	<0.00	4.89	0.81
Alluvium thickness	Grid 3	-0.13	-0.96	20.72	1.04
A-B interbed elevation	Grid 3	-0.74	<0.00	36.02	0.96
A-B interbed thickness	Grid 3	-0.28	34.60	13.79	1.76
B-C interbed elevation	Grid 2	-0.16	<0.00	9.74	0.98
B-C interbed thickness	Grid 2	-0.21	-0.63	56.08	1.71
C-D interbed elevation	Grid 0	-0.49	<0.00	57.39	1.24
C-D interbed thickness	Grid 0	0.00	1.87	101.24	1.16
C-D interbed elevation	Grid 1	0.14	<0.00	23.23	1.25
C-D interbed thickness	Grid 1	-0.35	-4.39	109.55	1.23

Cross validation was done for predictions made for the specified grid using the variogram for that grid and only for sample locations within that grid. Values in red font exceed the limit given in the text.

An important aspect of the hydrologic model is the lack of a specific interbed in a given area, which would retard flow if present. There are many locations where at least one of the interbeds was not found. Appropriately predicting these zero-thickness interbeds is important. As part of kriging model assessment, the distribution of measured interbed thickness is compared to predicted interbed thickness for locations within those grids to be used in the hydrologic model (see Figure 6). The predicted thickness values are generally more symmetric than the measured thickness values and have slightly smaller range. These predictions also predict zero thickness with lower frequency; some observed zero-thickness areas are not preserved in the predictions. This is because of the smoothing effect of kriging and because many zero-thickness locations have nonzero thickness locations nearby. The elevation distributions for measured and predicted values match well.

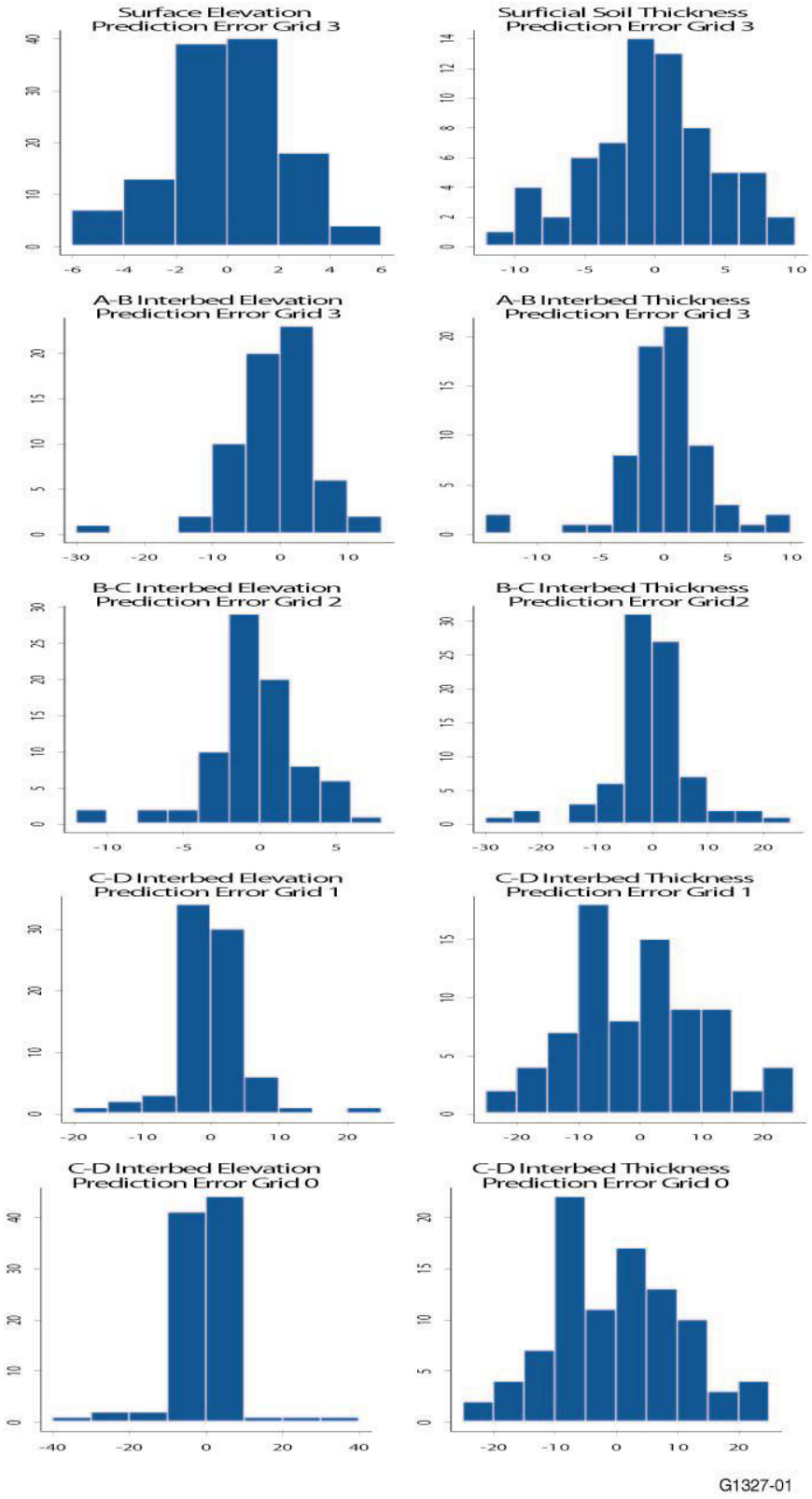

Figure 7. Histograms of cross-validation errors for layers and grids used in hydrologic modeling (surface through A-B interbed on Grid 3, B-C interbed on Grid 2, and C-D interbed on Grids 1 and 0).

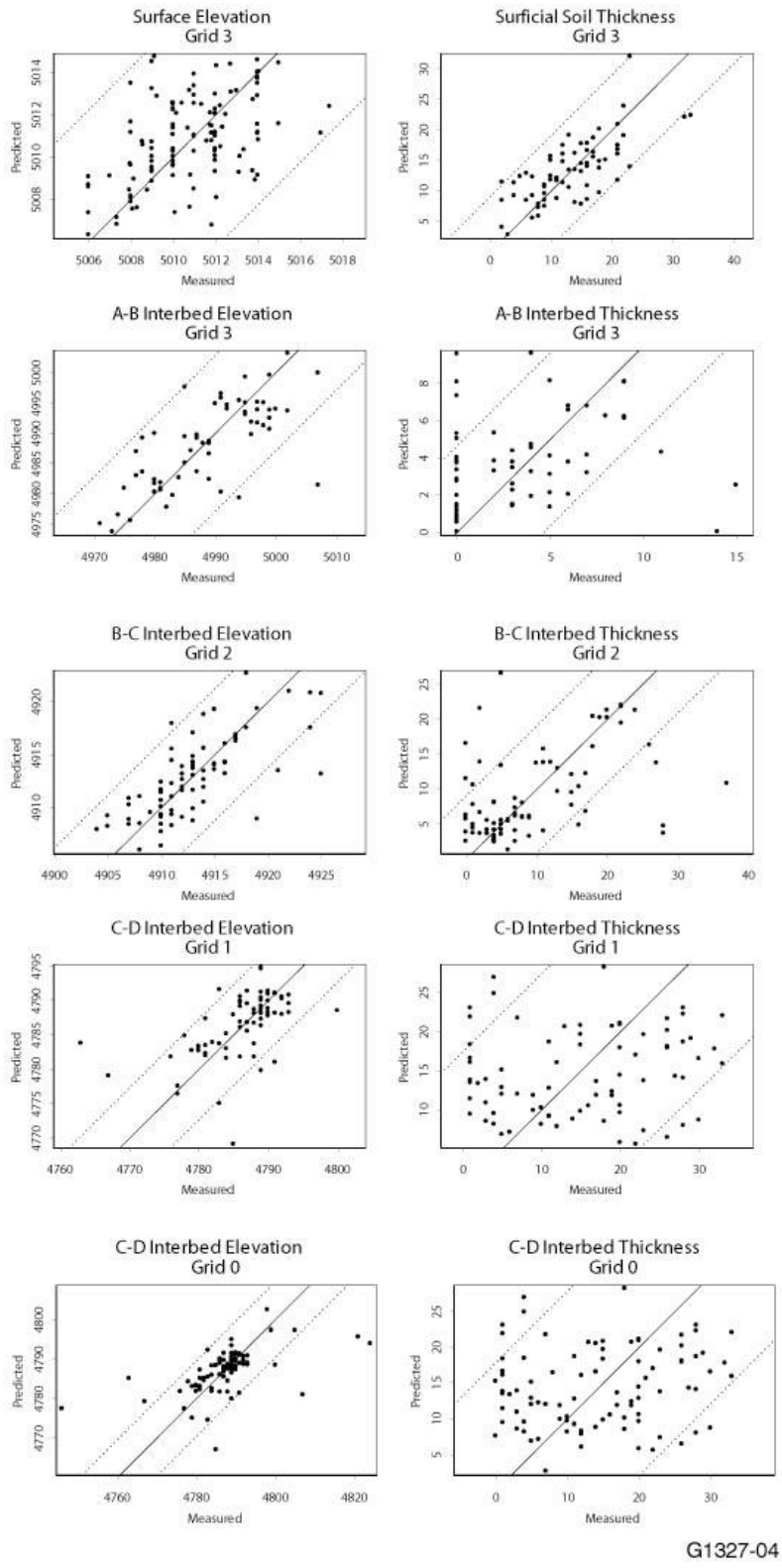

Figure 8. Measured values versus predicted values on grids used for hydrologic model.

6. DISCUSSION

The predictions presented here are updated from 2002 (Leecaster 2002). The predictions made then were based on fewer sample locations, single variograms used for all prediction grids, and inclusion of large-scale trends. There were 16 new sample locations available for this effort. The utility of these sample locations is more than just 16 locations; it adds a multitude of sample pairs that were used in the variogram modeling and kriging predictions. A thorough review of available lithologic data resulted in some revisions to previous lithologic selections as a result of relying more on geophysical interpretations than on drillers' logs (Ansley, Helm-Clark, and Magnuson 2004). These updated interpretations were used in this effort.

The variograms used in *Geostatistic Modeling in the RWMC Region* (Leecaster 2002) were based on a maximum distance of 3,000 ft and were all single-structure variograms. This approach did not take advantage of the structures in the variogram or the prediction grid differences. As a result, the predictions are oversmoothed and did not reflect the zero-thickness interbeds in the data. A large-scale trend was fit to the data in *Geostatistic Modeling in the RWMC Region* (Leecaster 2002). During a reassessment of this trend, it was considered to be an artifact of the sample locations. Many samples are taken within the SDA and fewer at greater distances from the SDA. These far-away locations tend to be in the northeast and southwest directions from the SDA, following the aquifer flow pattern. These far-distant values produce an arbitrary trend that may or may not reflect reality. Given more data in outlying areas, this trend, or lack thereof, could be determined accurately.

Predictions for the C-D interbed thickness did not match up well with the data, as discussed. There are fewer data points (n = 106) to use in the kriging model for this interbed. This affects calculation of the empirical variogram, the model of the variogram, and the kriging predictions themselves. The variogram at close distance is quite large compared to that for other layers and to the asymptotic variance (see Table 3). This creates a prediction that is closer to an overall mean because sample values are weighted more evenly. This layer, especially, should be the subject of a sensitivity analysis for the hydrologic model.

Kriging was performed on data reported on alternate elevation and thickness values. The predictions were compared to those performed on all elevations, but these produced a greater overlap problem due to the greater variability inherent in the larger values (elevation in thousands versus thickness in tens). A rigorous comparison was made in *Geostatistic Modeling in the RWMC Region* (Leecaster 2002). Although the predictions were similar, those using the thickness values were preferred because they produced a rougher surface.

The kriging standard deviations indicate that the precision of the predictions is good overall, given the small number of sample site locations (see Table 5 and Appendix B). The standard errors should be taken into account when using the predictions. Hydrologic models based on these predictions should take into account their uncertainty. For predictions that have a large standard error, the end predictions may not be deemed useful because of their combined model uncertainty. The kriging model standard deviations are given in Table 5. The location of future spatial modeling also is a factor. The prediction standard deviation is smaller in areas of dense sampling; therefore, future spatial modeling also will be more precise in these areas. Another approach to assessing kriging model uncertainty is to generate a large set of realizations using spatial conditional simulation. This is a useful technique for sensitivity and uncertainty analysis for the hydrologic model.

Table 5. Kriging model standard error for layers and grids used in the hydrologic model.

Variable	Grid	Minimum Standard Error	Maximum Standard Error	Mean Standard Error
Surface elevation	3	0.97	6.33	3.26
Surficial soil thickness	3	1.56	6.77	5.00
A-B interbed elevation	3	2.33	8.69	6.51
A-B interbed soil thickness	3	0.89	2.78	2.12
B-C interbed elevation	2	1.14	5.06	3.13
B-C interbed soil thickness	2	1.65	8.08	4.76
C-D interbed elevation	1	1.36	6.38	3.76
C-D interbed soil thickness	1	3.26	10.03	7.41
C-D interbed elevation	0	1.68	13.23	10.04
C-D interbed soil thickness	0	4.16	7.33	6.05

Problems in spatial modeling these data include general sparseness of sample locations as well as large distances between many of the sites; thus, predictions were made over a large area without ample coverage. These problems affected all spatial modeling steps from calculating the variogram to kriging predictions and standard errors. The variogram model is most dependent on the fitting at small distances because that is where the differences occur relative to model shape and nugget. Beyond the range, the variogram is of little use. Therefore, the pairs of points within the small distances are important. The variogram model parameters are used to predict values at unsampled locations as well as to estimate the variance of the predictions; therefore, these also are most affected by the variogram model at small ranges. Because the weights in the kriging equations change (sometimes drastically) from close distances to the range, these values can greatly affect the predictions. The predictions also will vary depending on the form of the variogram model at small distances. For instance, the Gaussian and spherical models have different shapes at small distances. The Gaussian model starts horizontally and then slopes upward, producing a surface that is quite smooth because close sites are predicted to be similar. The spherical model starts with an upward slope, producing a surface that is rougher because close sites can be predicted to show more difference. For these reasons, it is essential that sites in the area of interest be close together. Sparse sites will produce predictions that may be biased because of inaccurate variogram modeling as well as predictions that have large variances. Therefore, little confidence is placed in those values.

7. REFERENCES

Aero-Graphics, 2000, "Topographic Mapping of the Radioactive Waste Management Complex Area at the Idaho National Engineering and Environmental Laboratory," Aero-Graphics, Inc.

Ansley, Shannon L., Catherine M. Helm-Clark, and Swen O. Magnuson, 2004, *Updated Stratigraphic Selections for Wells in the Vicinity of the Subsurface Disposal Area,* ICP/EXT-04-00207, Rev. 0, Idaho Completion Project.

Cressie, N. and D. M. Hawkins, 1980, "Robust Estimation of the Variogram, I," *Journal of the International Association for Mathematical Geology*, Vol. 12, pp. 115–125.

Deutsch, C. V. and A. G. Journel, 2000, *GSLIB: Geostatistical Software Library and User's Guide*, New York: Oxford University Press.

DOE-ID, 1991, *Federal Facility Agreement and Consent Order for the Idaho National Engineering Laboratory,* Administrative Docket No. 1088-06-29-120, U.S. Department of Energy Idaho Operations Office; U.S. Environmental Protection Agency, Region 10; and Idaho Department of Health and Welfare.

Goovaerts, Pierre, 1997, *Geostatistics for Natural Resources Evaluation*, London: Oxford University Press.

Leecaster, Molly K., 2002, *Geostatistic Modeling of Subsurface Characteristics in the Radioactive Waste Management Complex Region, Operable Unit 7-13/14*, INEEL/EXT-02-00029, Rev. 0, Idaho National Engineering and Environmental Laboratory.

Magnuson, S. O. and A. J. Sondrup, 1998, *Development, Calibration, and Predictive Results of a Simulator for Subsurface Pathway Fate and Transport of Aqueous- and Gaseous-Phase Contaminants in the Subsurface Disposal Area at the Idaho National Engineering and Environmental Laboratory*, INEEL/EXT-97-00609, Idaho National Engineering and Environmental Laboratory.

Matheron, G., 1963, "Principles of Geostatistics," *Economic Geology*, Vol. 58, pp. 1246–1266.

S+SPATIALSTATS, Version 1.5, Seattle, Washington: Insightful Corporation, 2000.

Appendix A

Directional Variograms and Omni-Directional Variogram with Model

Appendix A

Directional Variograms and Omni-Directional Variogram with Model

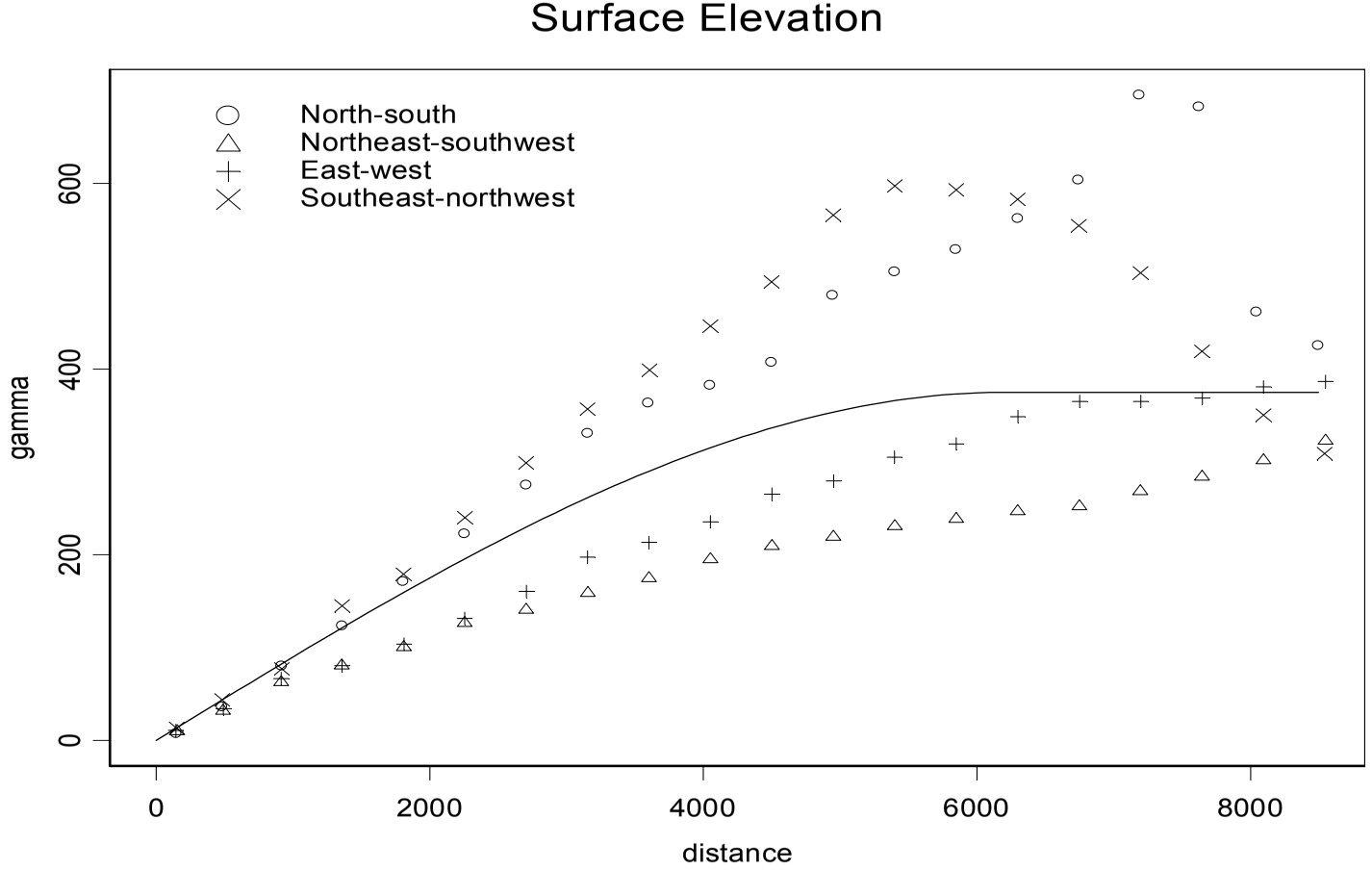

Figure A-1. Directional variograms for surface elevation.

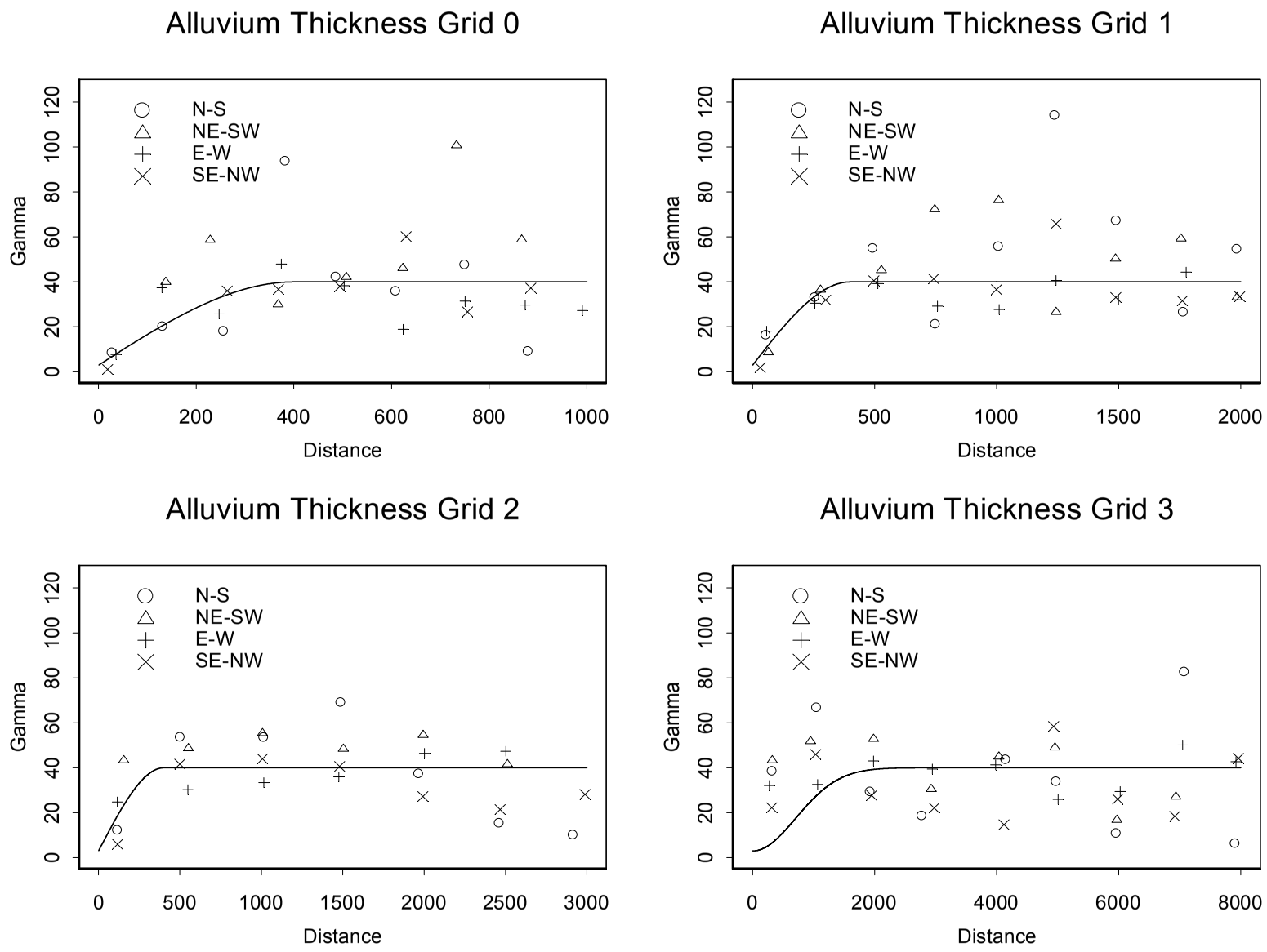

Figure A-2. Directional variograms for alluvium thickness on four prediction grids.

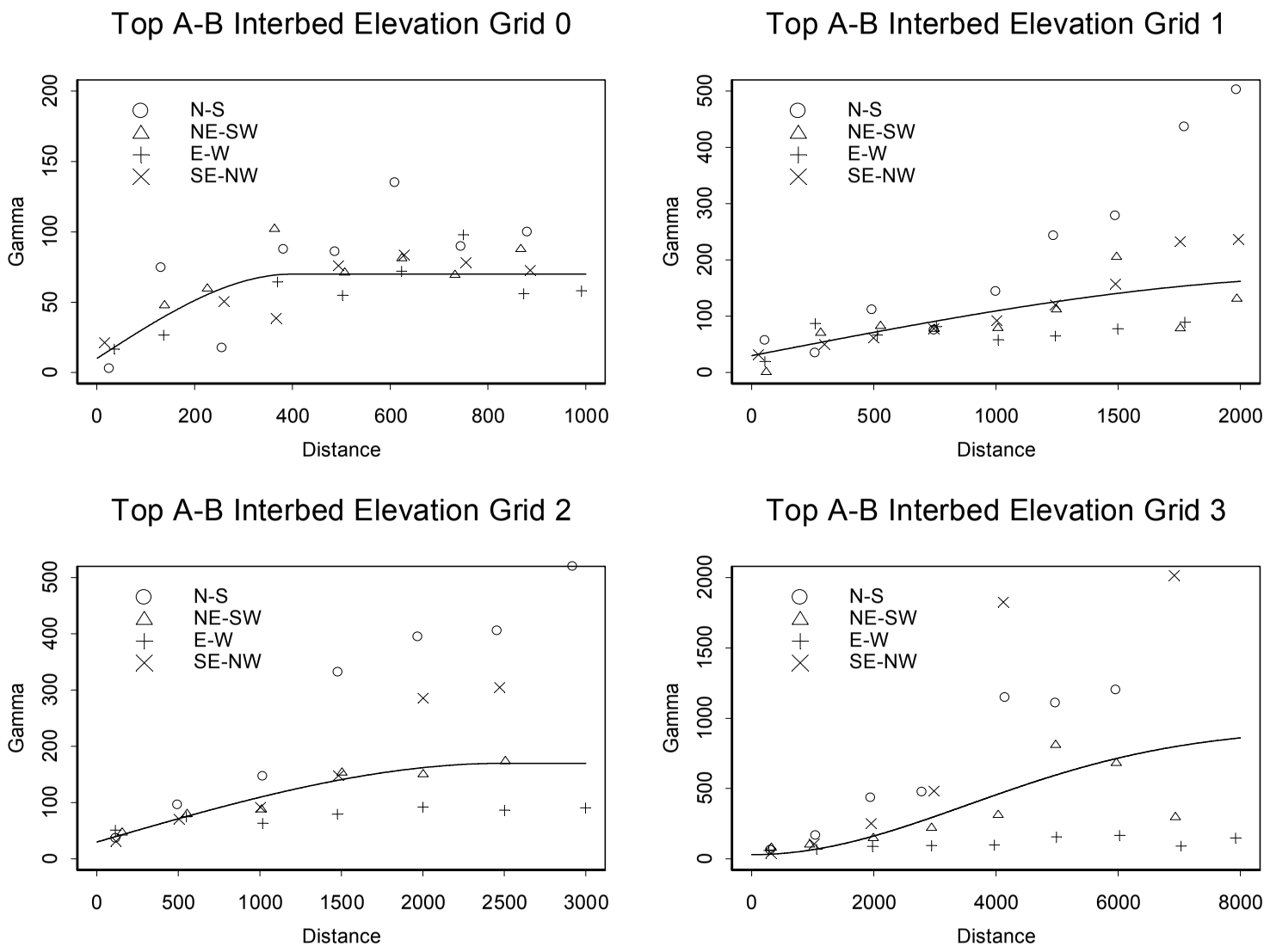

Figure A-3. Directional variograms for A-B interbed elevation on four prediction grids.

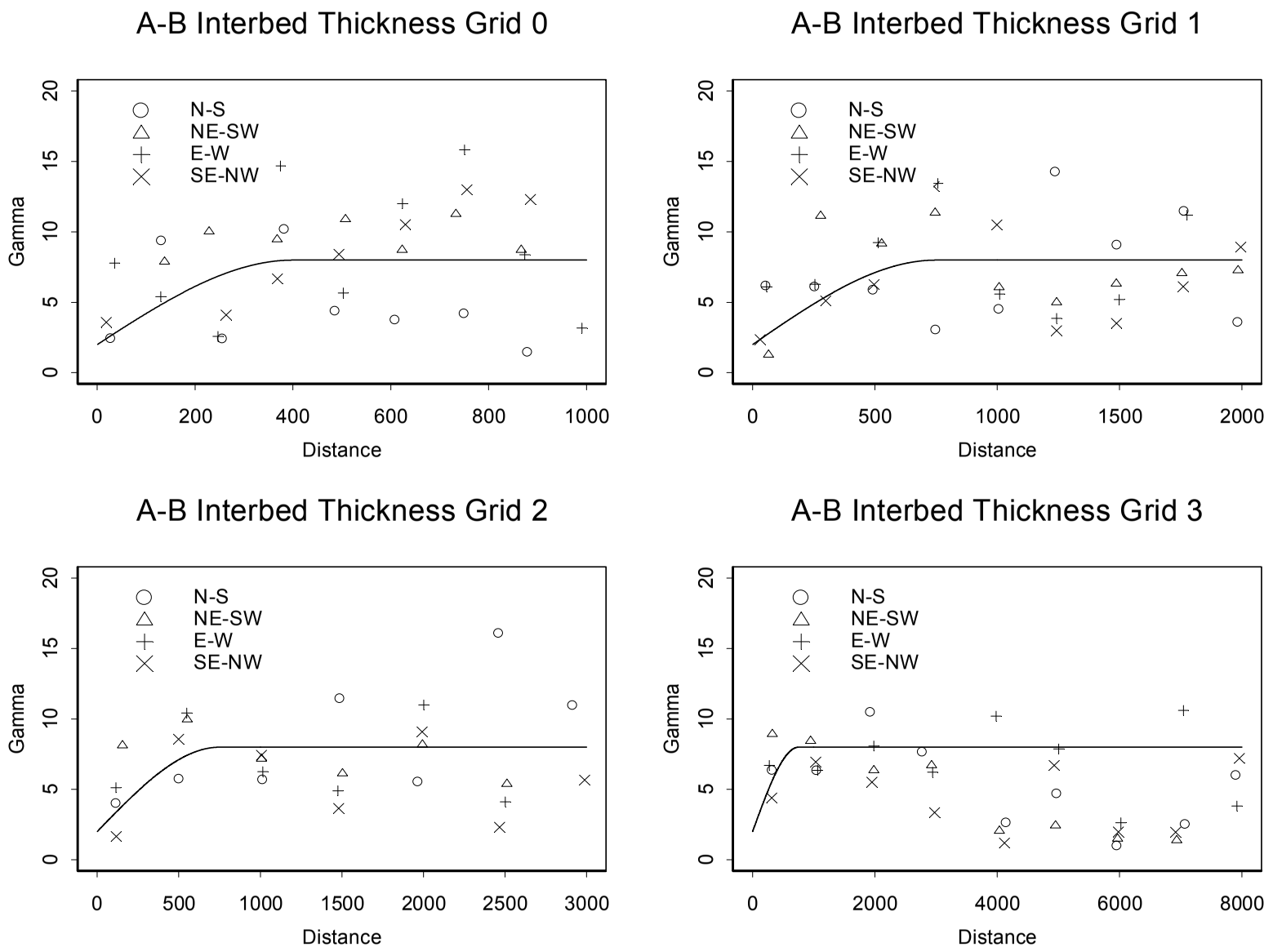

Figure A-4. Directional variograms for A-B interbed thickness on four prediction grids.

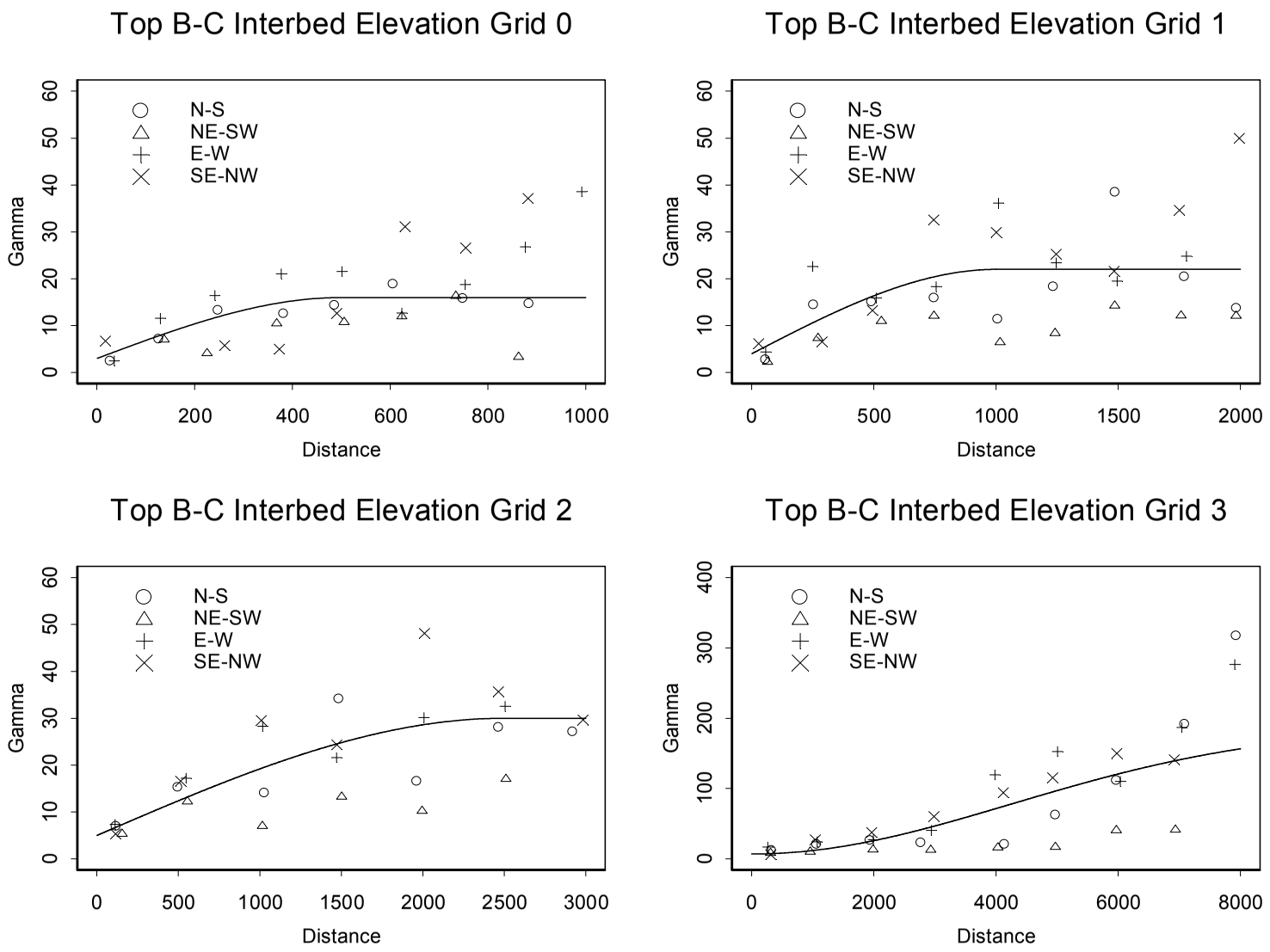

Figure A-5. Directional variograms for B-C interbed elevation on four prediction grids.

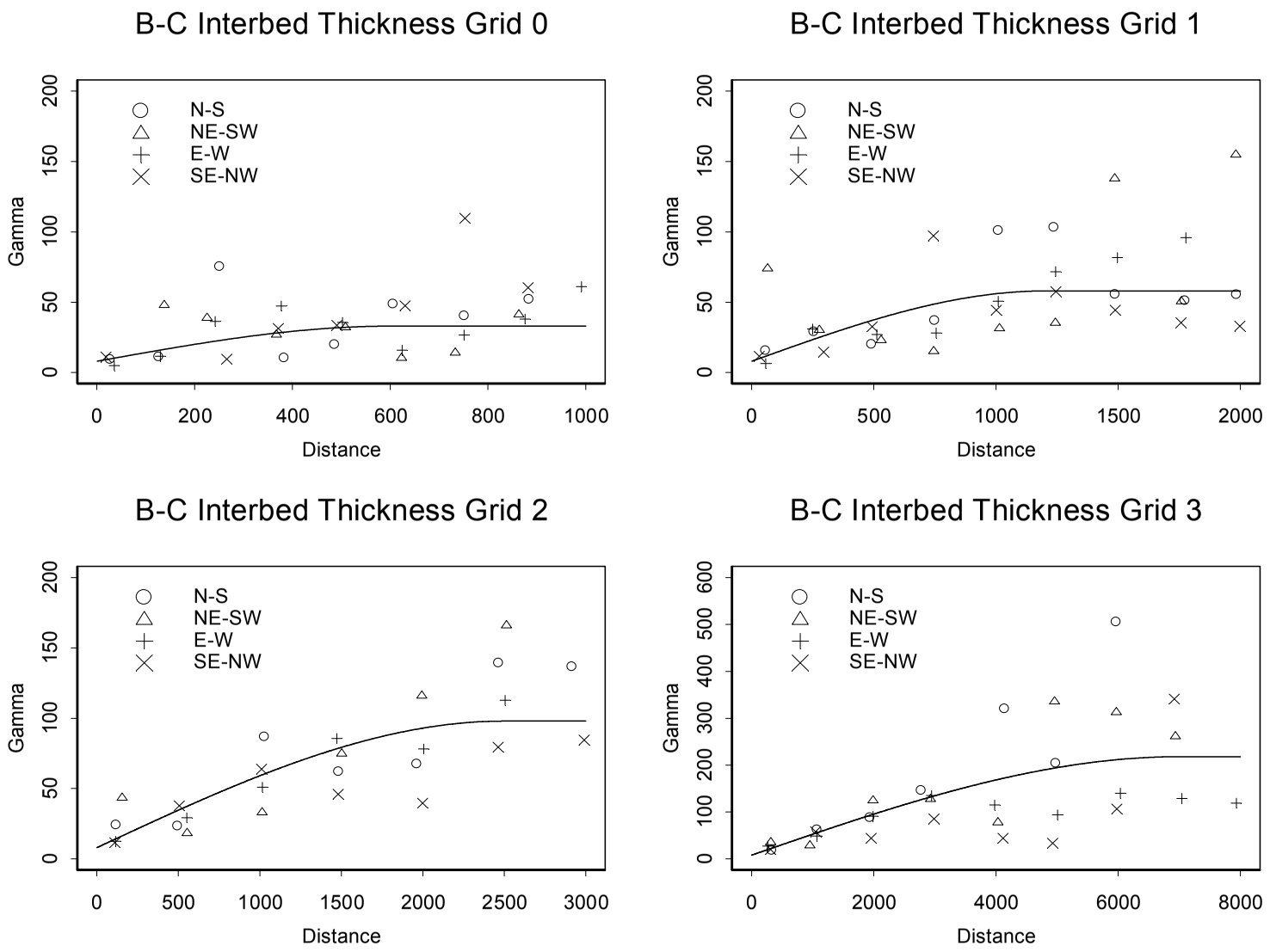

Figure A-6. Directional variograms for B-C interbed thickness on four prediction grids.

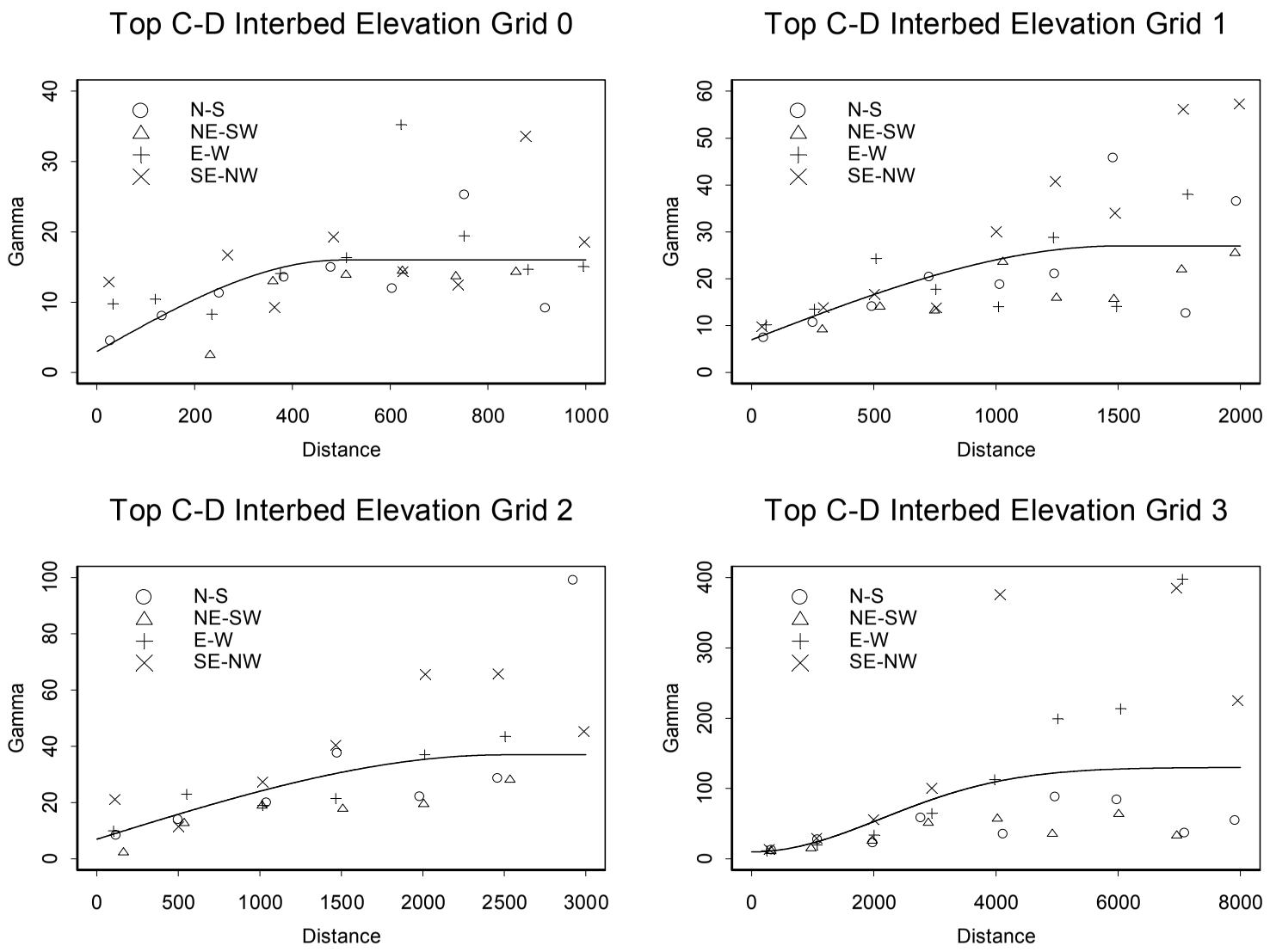

Figure A-7. Directional variograms for C-D interbed elevation on four prediction grids.

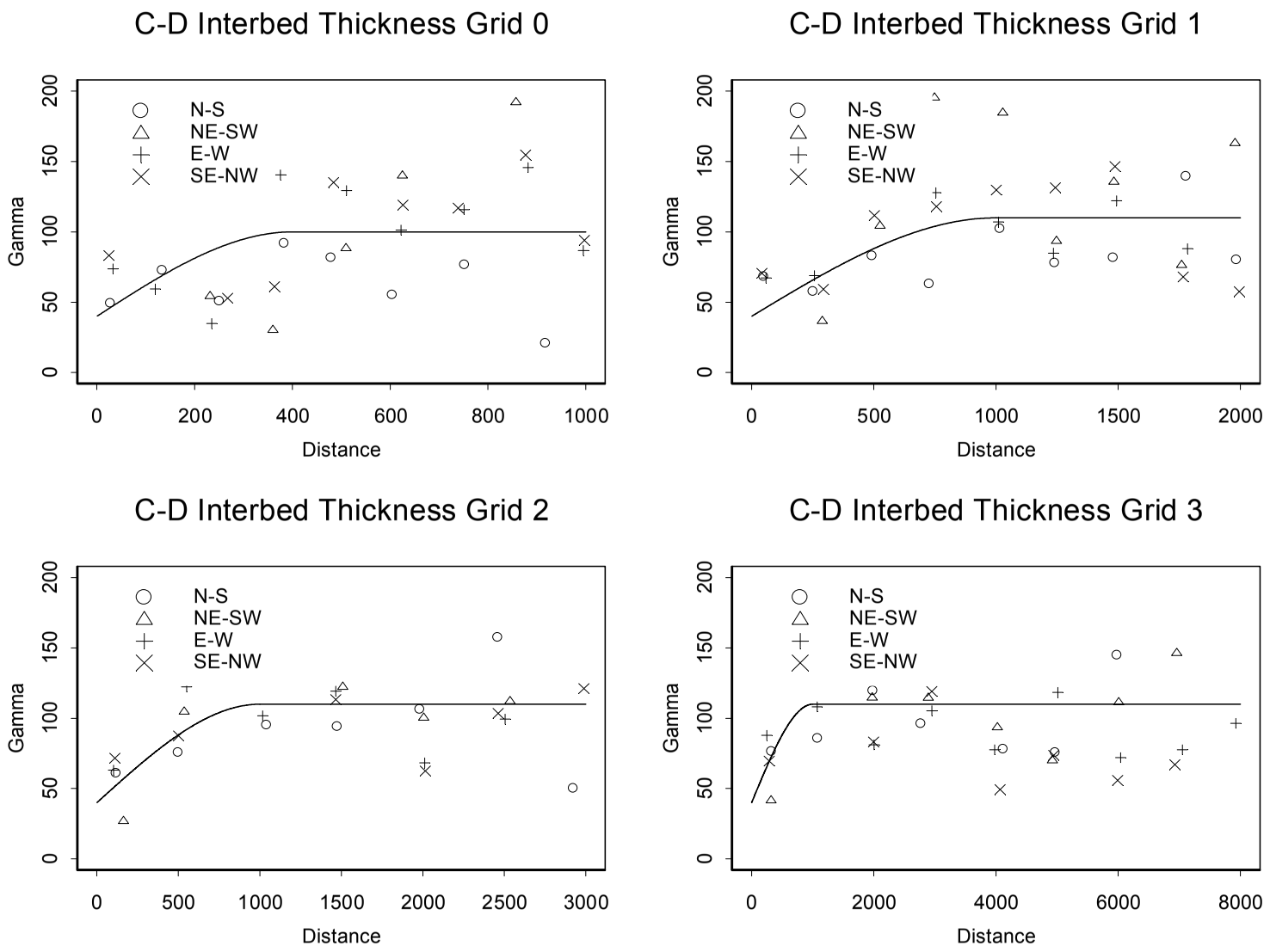

Figure A-8. Directional variograms for C-D interbed thickness on four prediction grids.

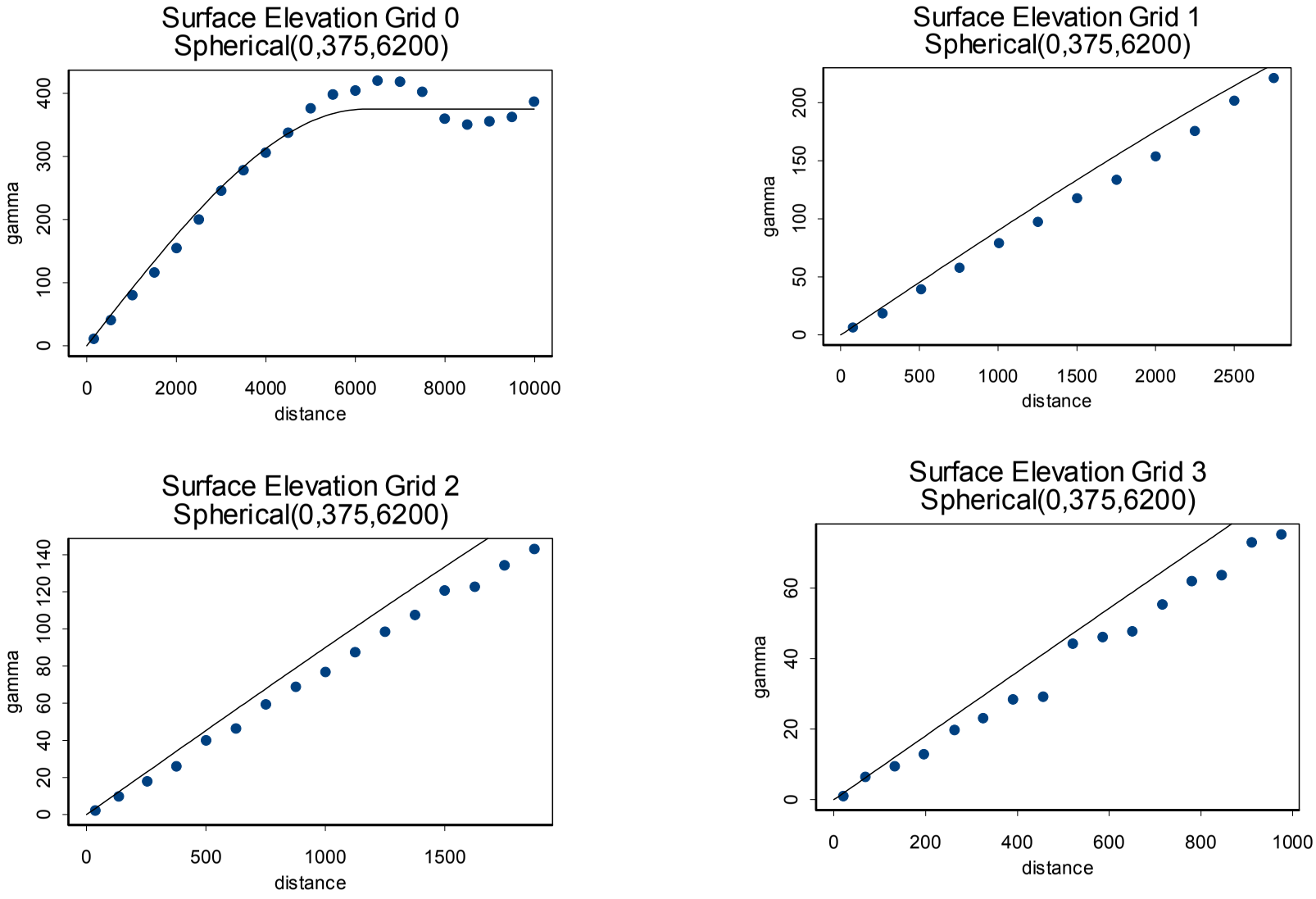

Figure A-9. Omni-directional variograms and models for surface elevation on four prediction grids.

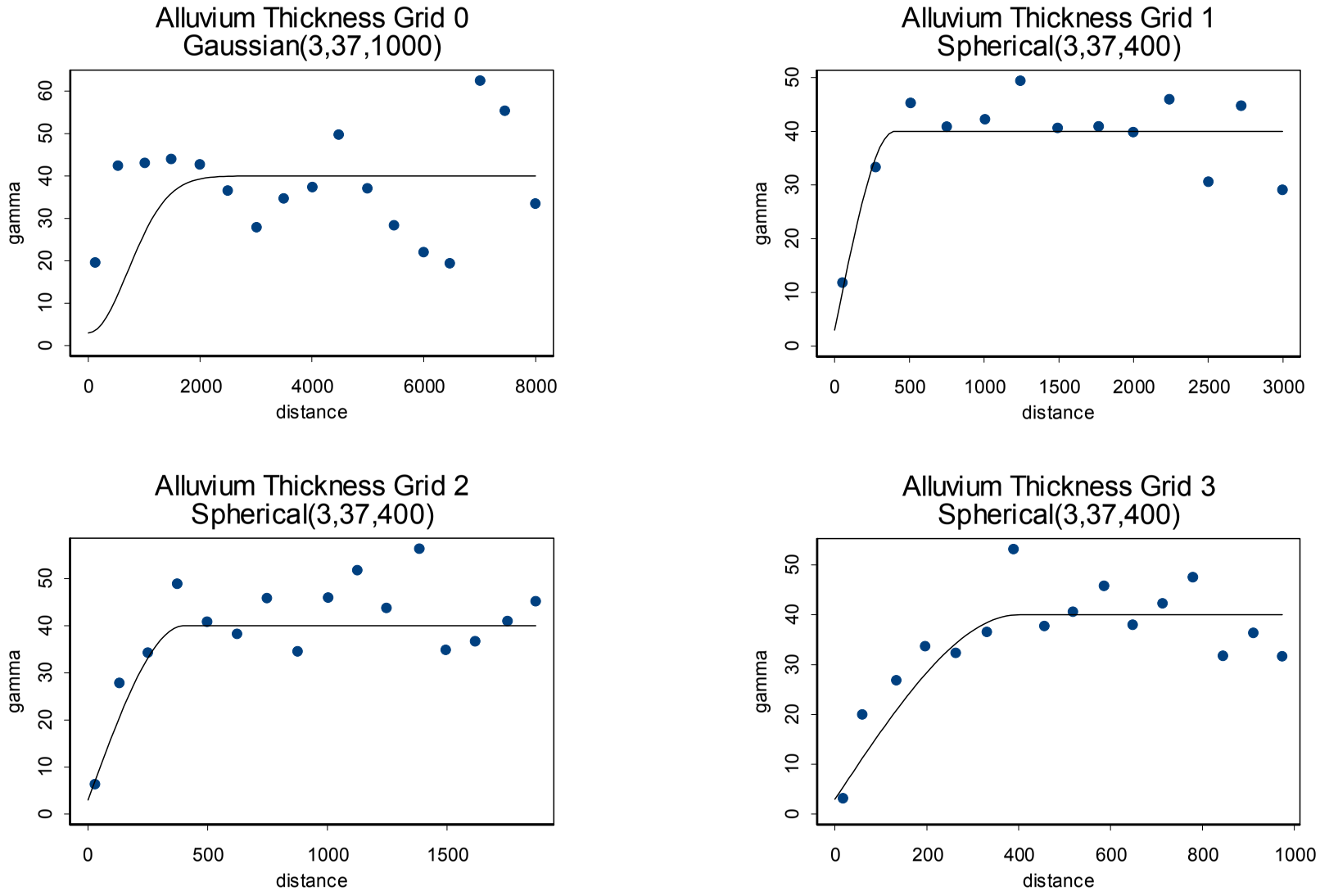

Figure A-10. Omni-directional variograms and models for alluvium thickness on four prediction grids.

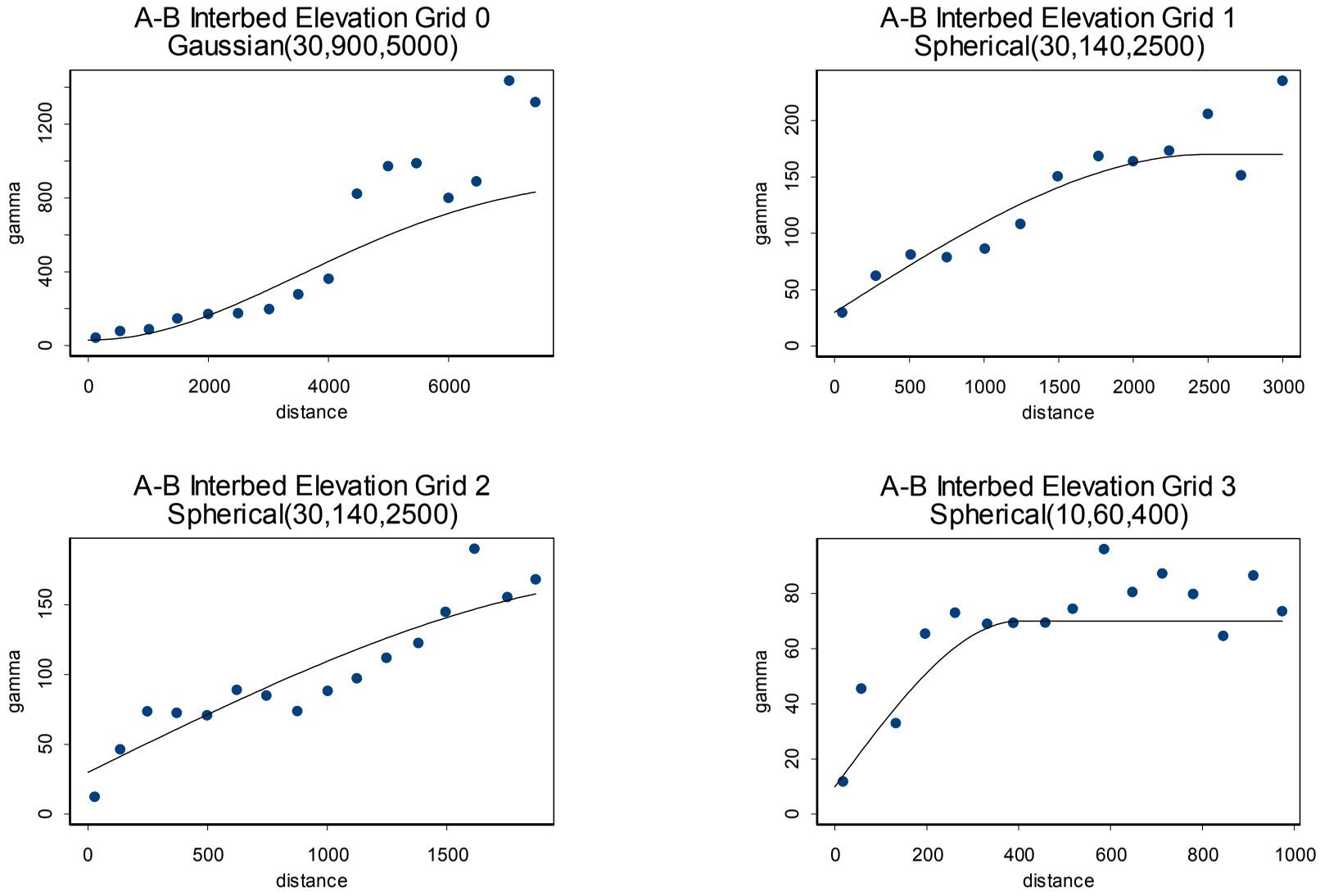

Figure A-11. Omni-directional variograms and models for A-B interbed elevation on four prediction grids.

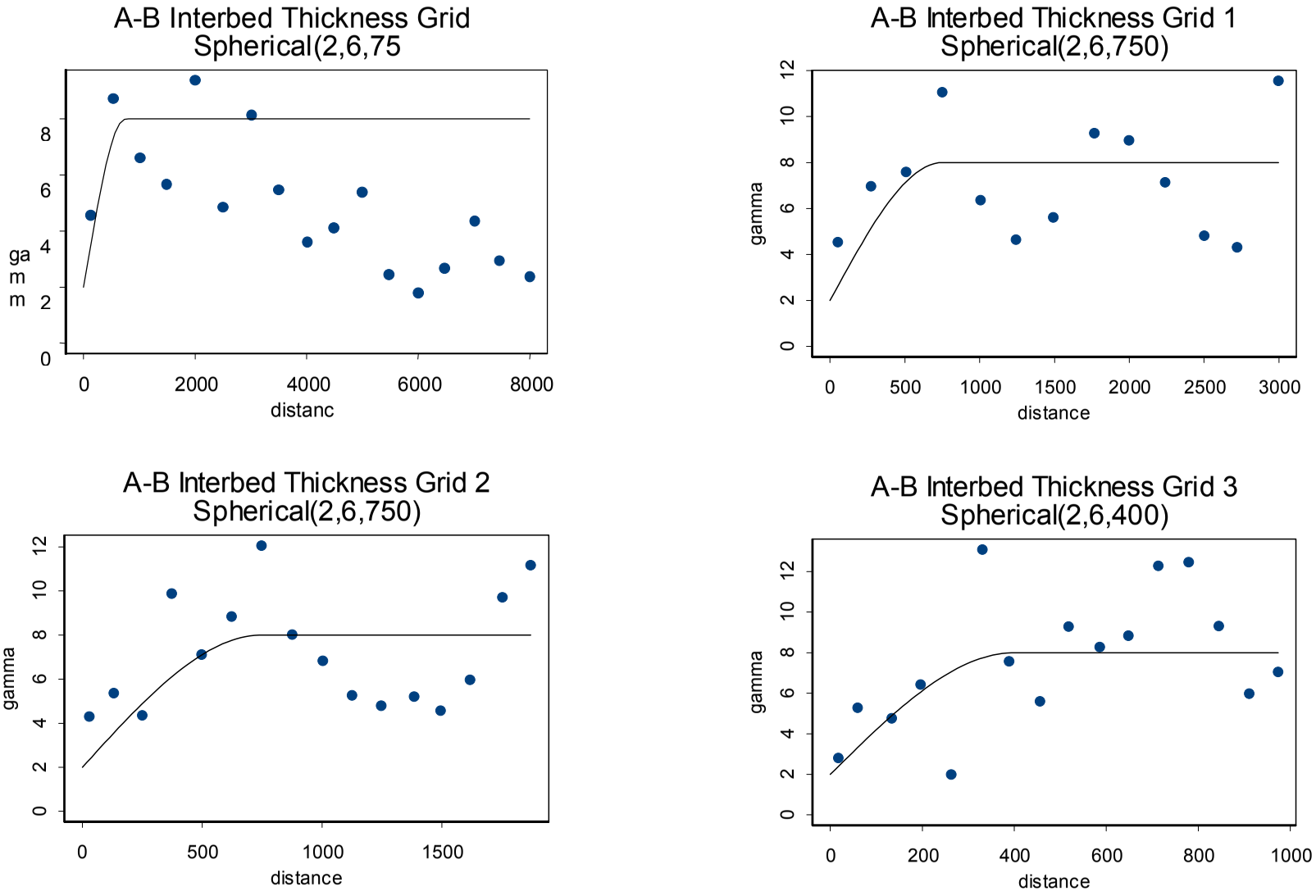

Figure A-12. Omni-directional variograms and models for A-B interbed thickness on four prediction grids.

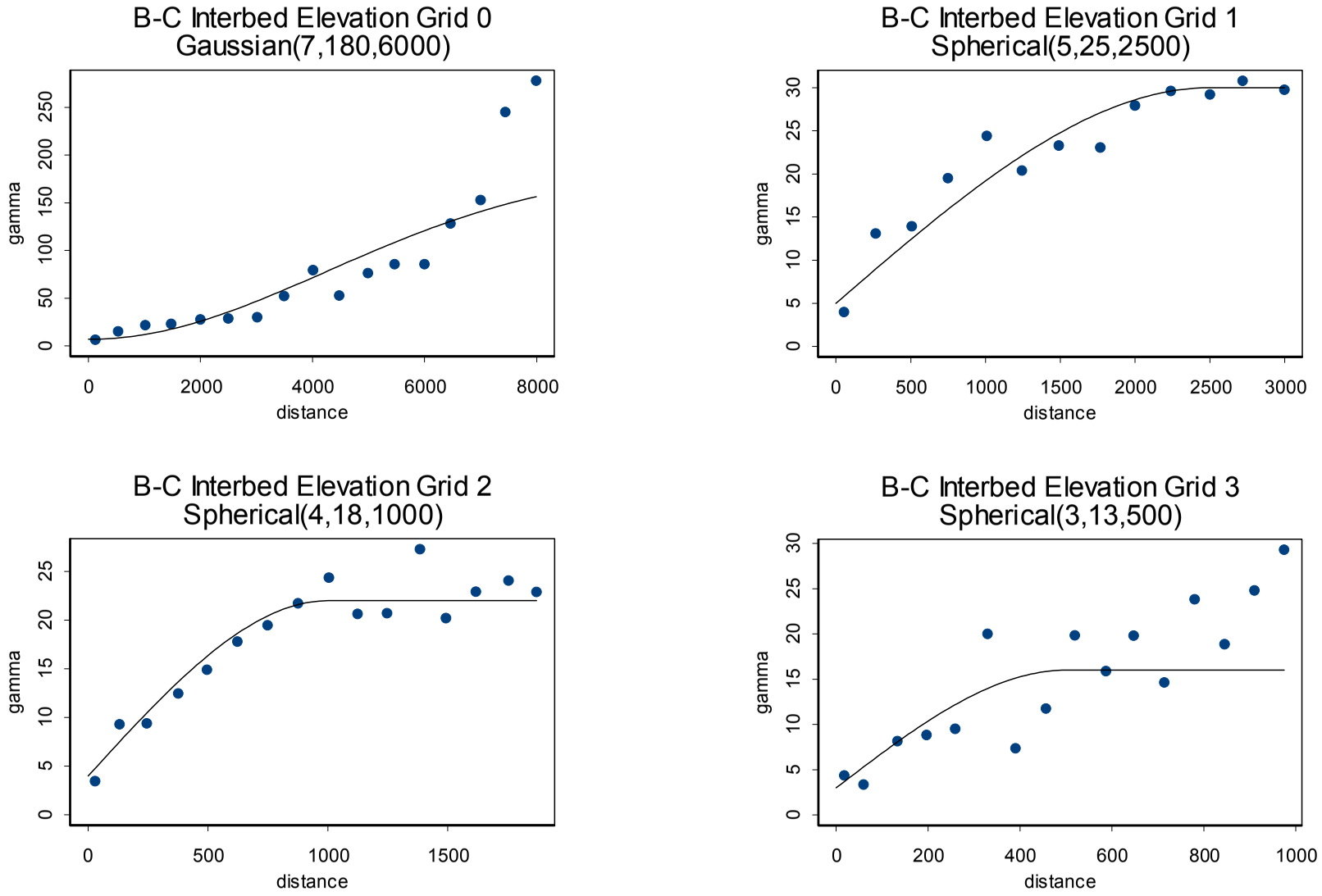

Figure A-13. Omni-directional variograms and models for B-C interbed elevation on four prediction grids.

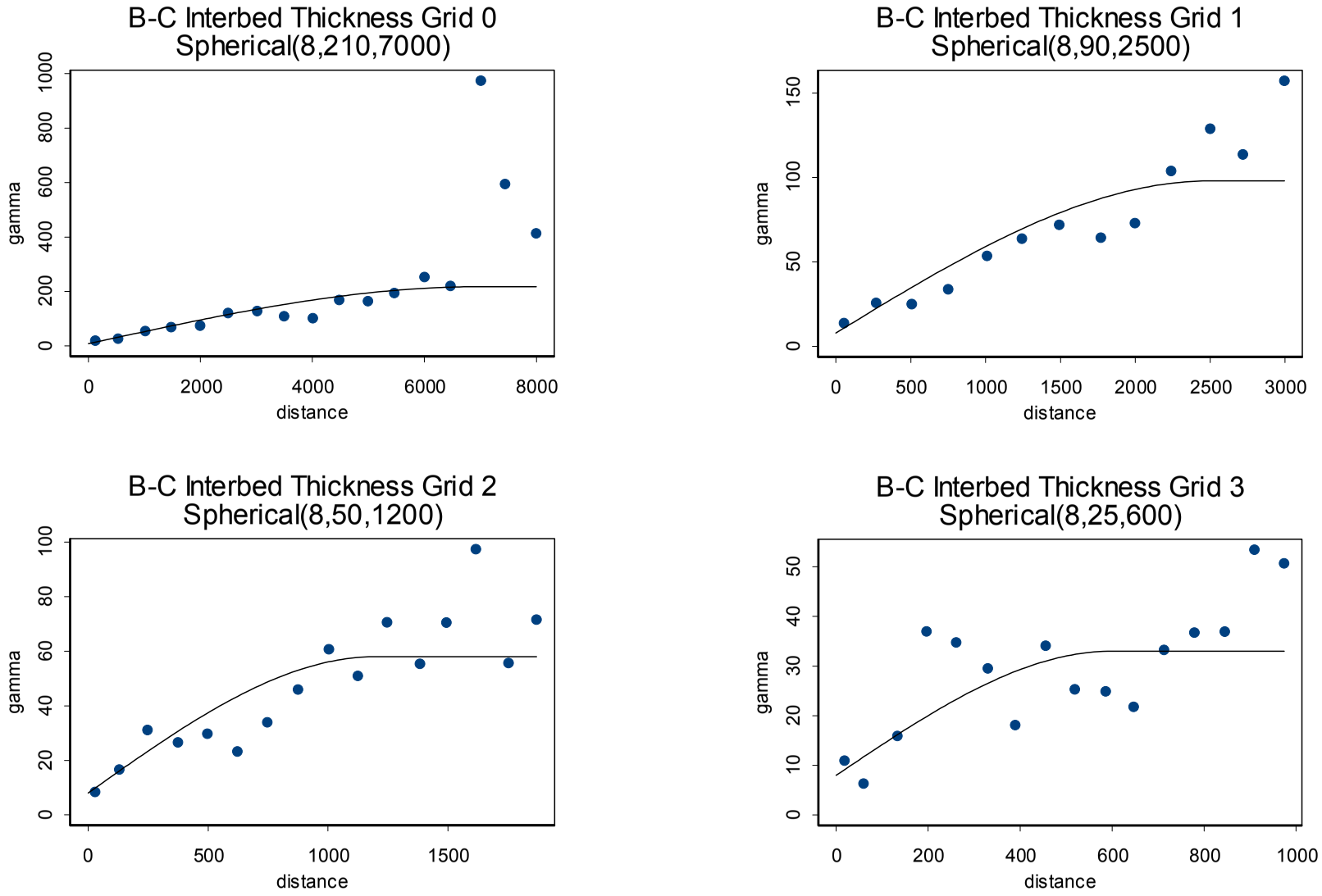

Figure A-14. Omni-directional variograms and models for B-C interbed thickness on four prediction grids.

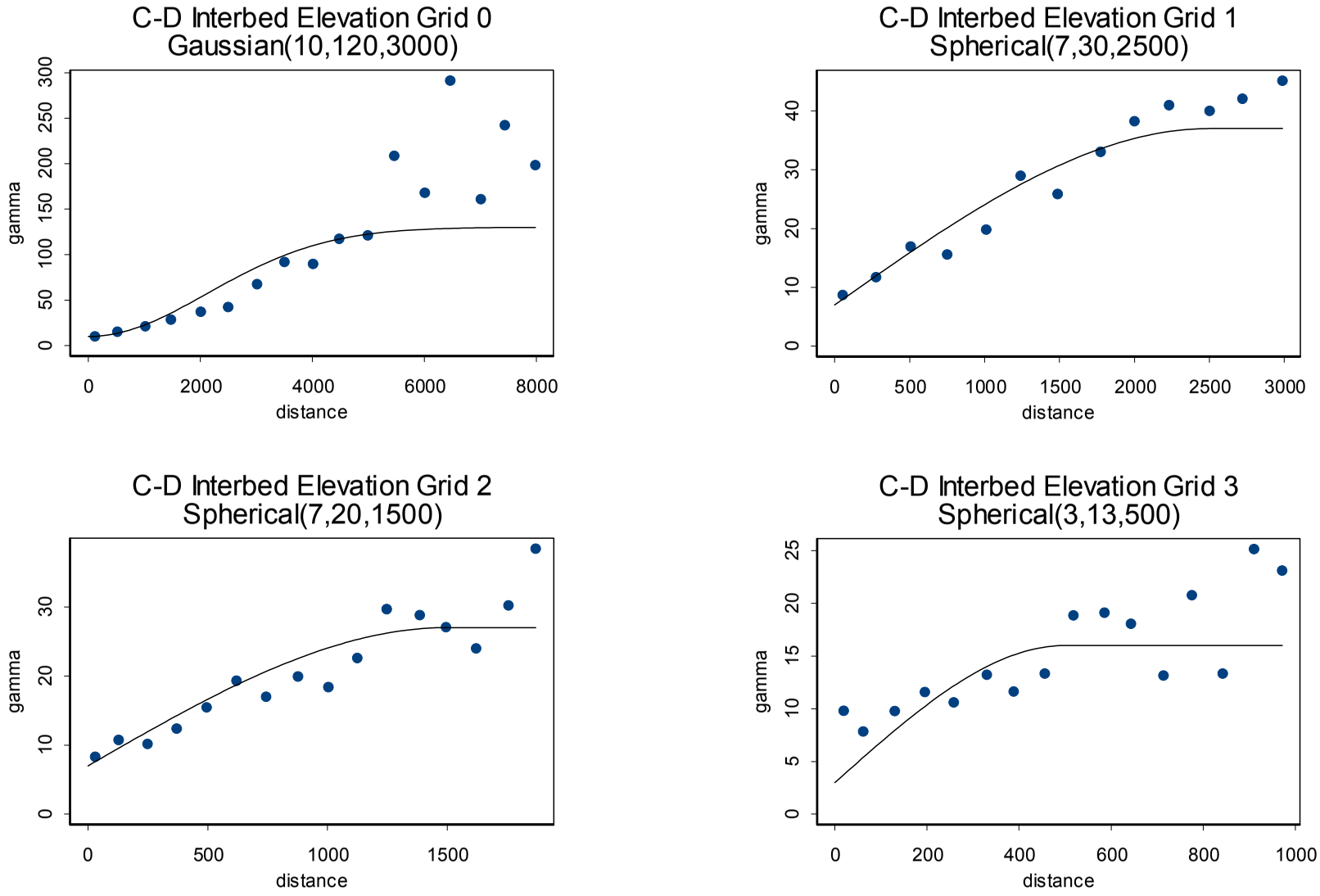

Figure A-15. Omni-directional variograms and models for C-D interbed elevation on four prediction grids.

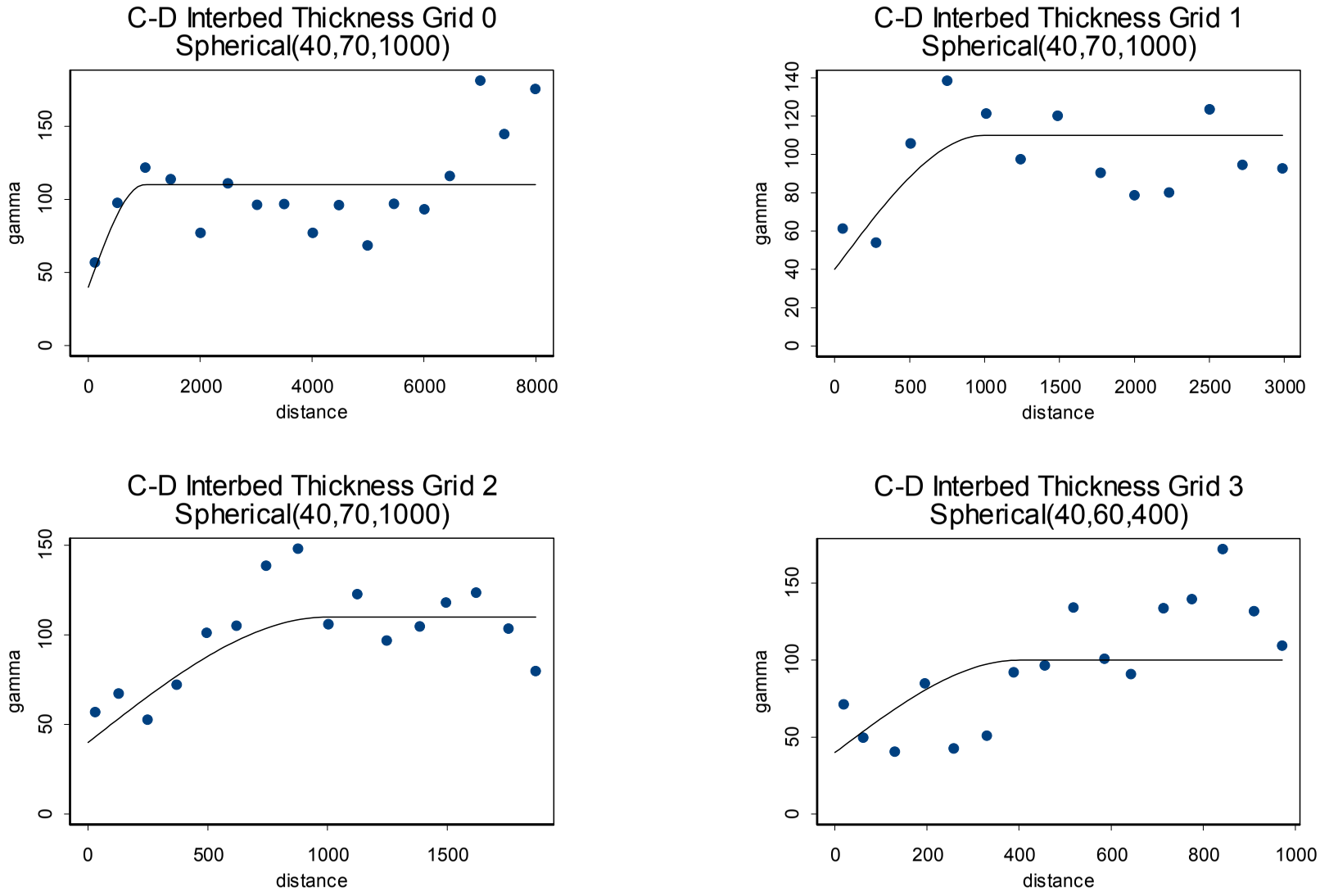

Figure A-16. Omni-directional variograms and models for C-D interbed thickness on four prediction grids.

Appendix B

Kriging Results and Standard Errors

Appendix B

Kriging Results and Standard Errors

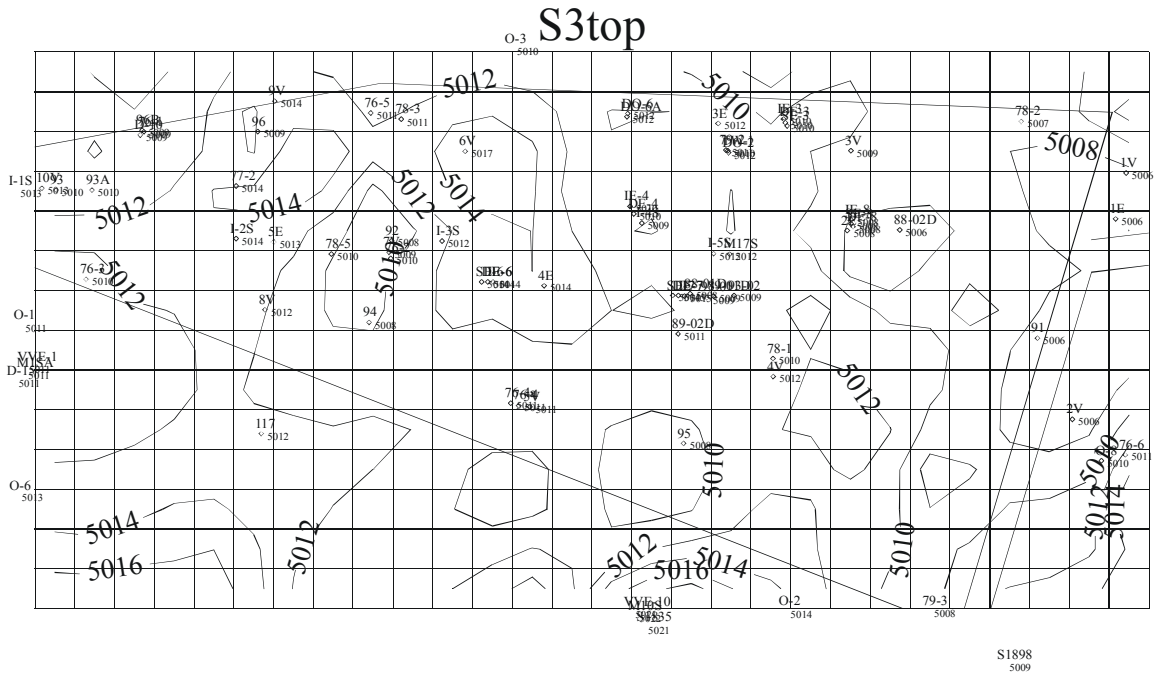

Figure B-1. Kriged surficial sediment top elevation (feet) for Grid 3.

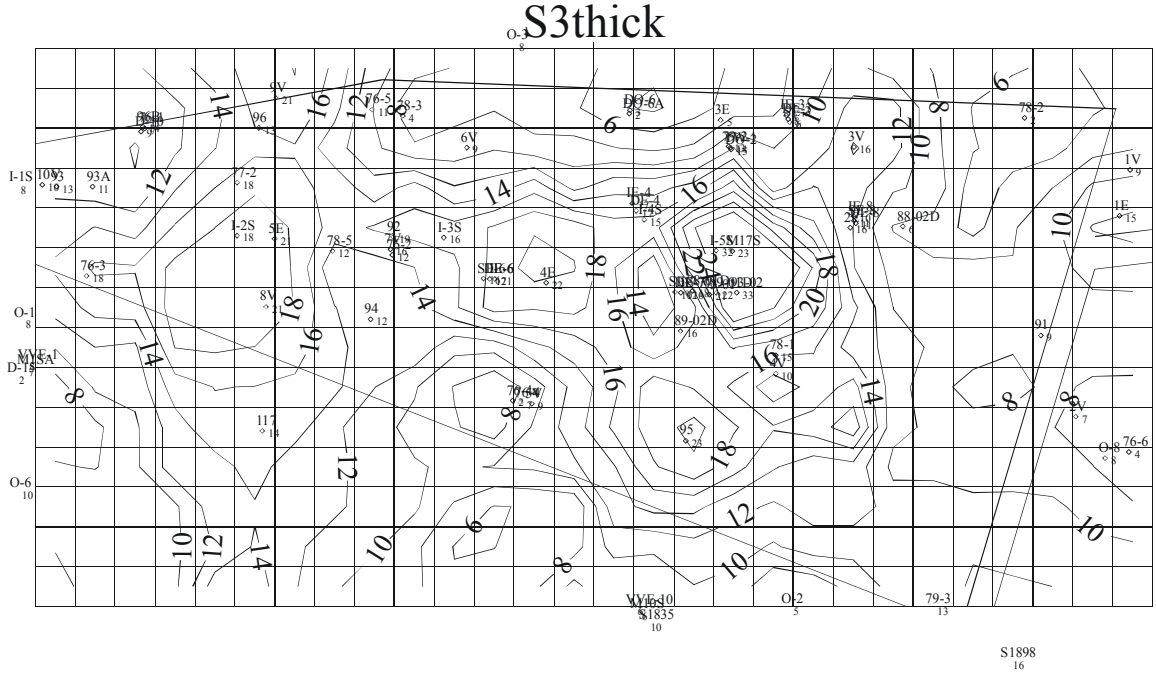

Figure B-2. Kriged surficial sediment thickness (feet) for Grid 3.

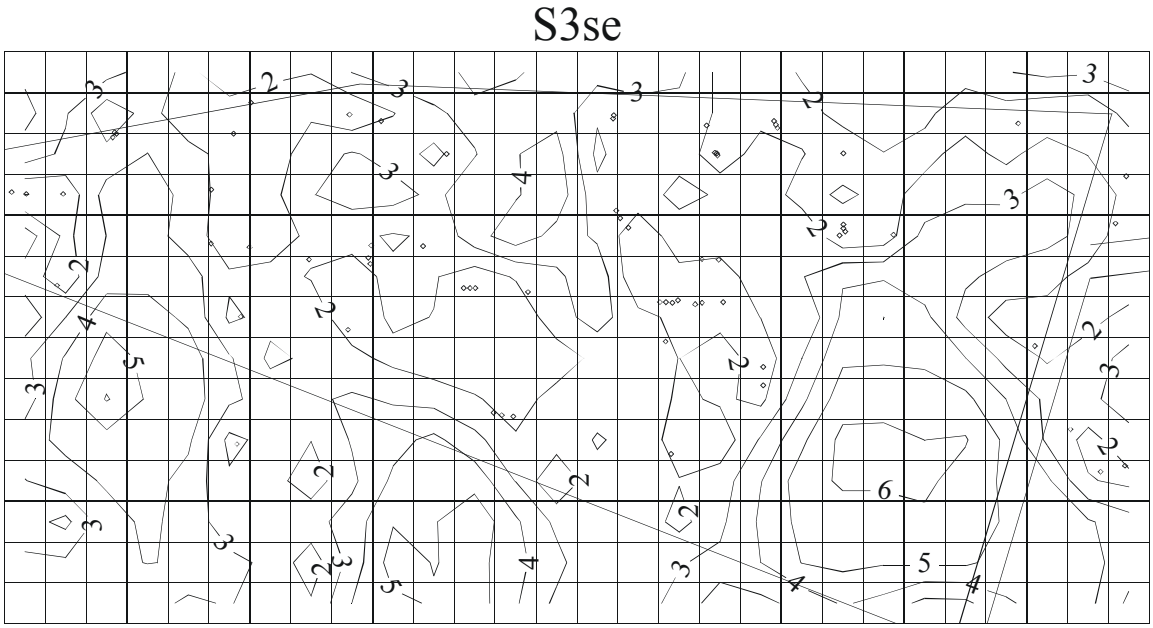

Figure B-3. Kriged surficial sediment top elevation standard error (feet) for Grid 3.

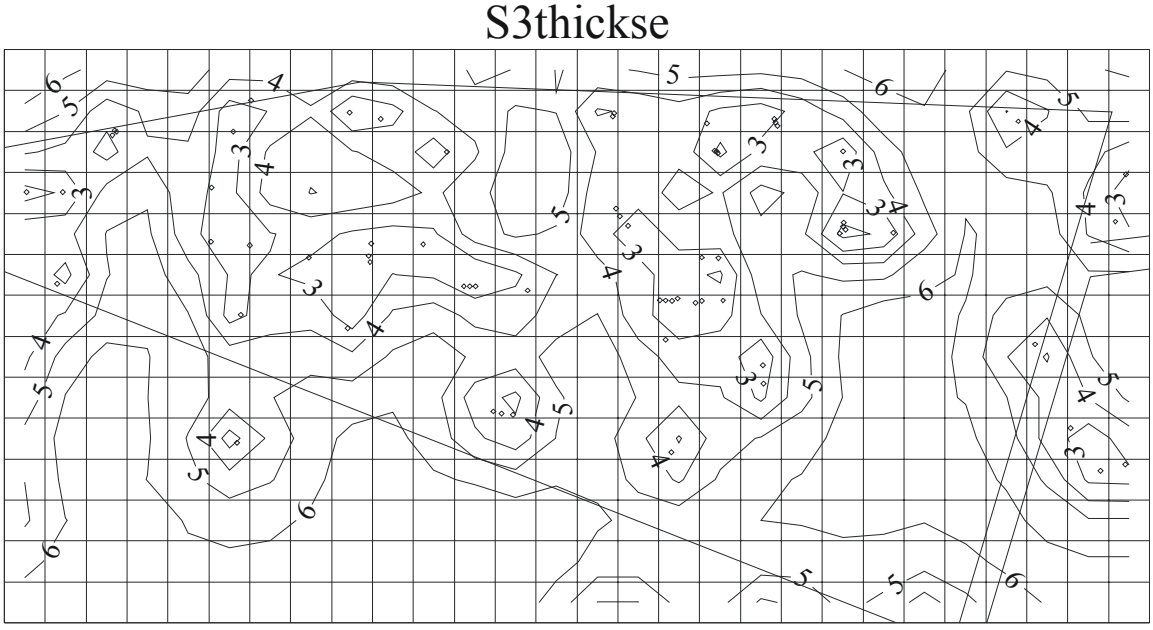

Figure B-4. Kriged surficial sediment thickness standard error (feet) for Grid 3.

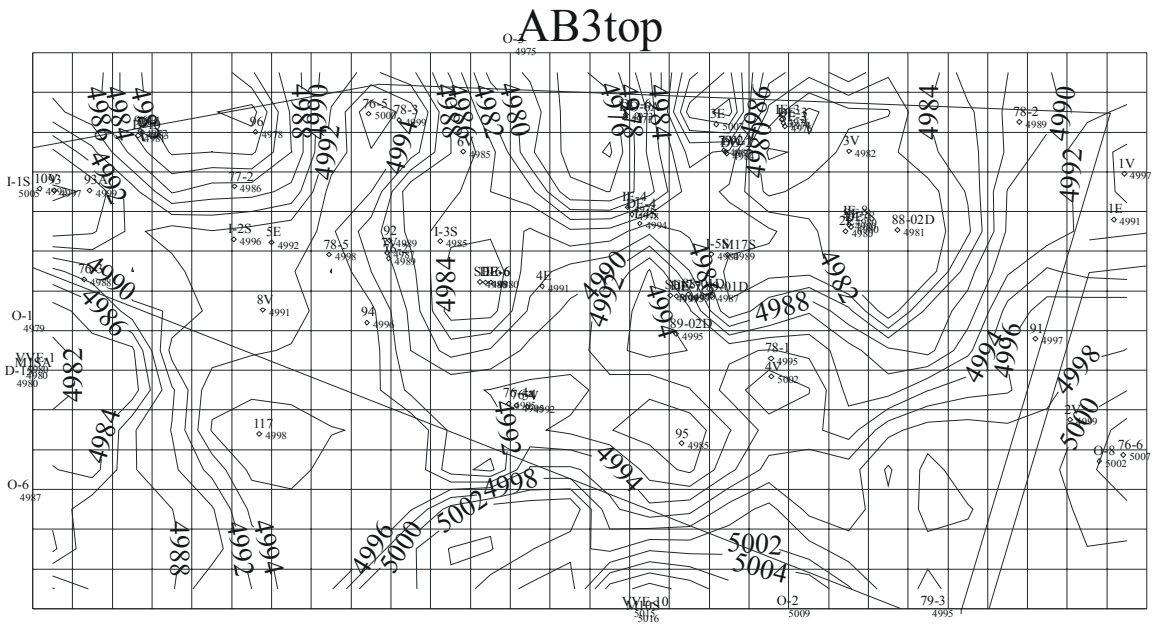

Figure B-5. Kriged A-B interbed top elevation (feet) for Grid 3.

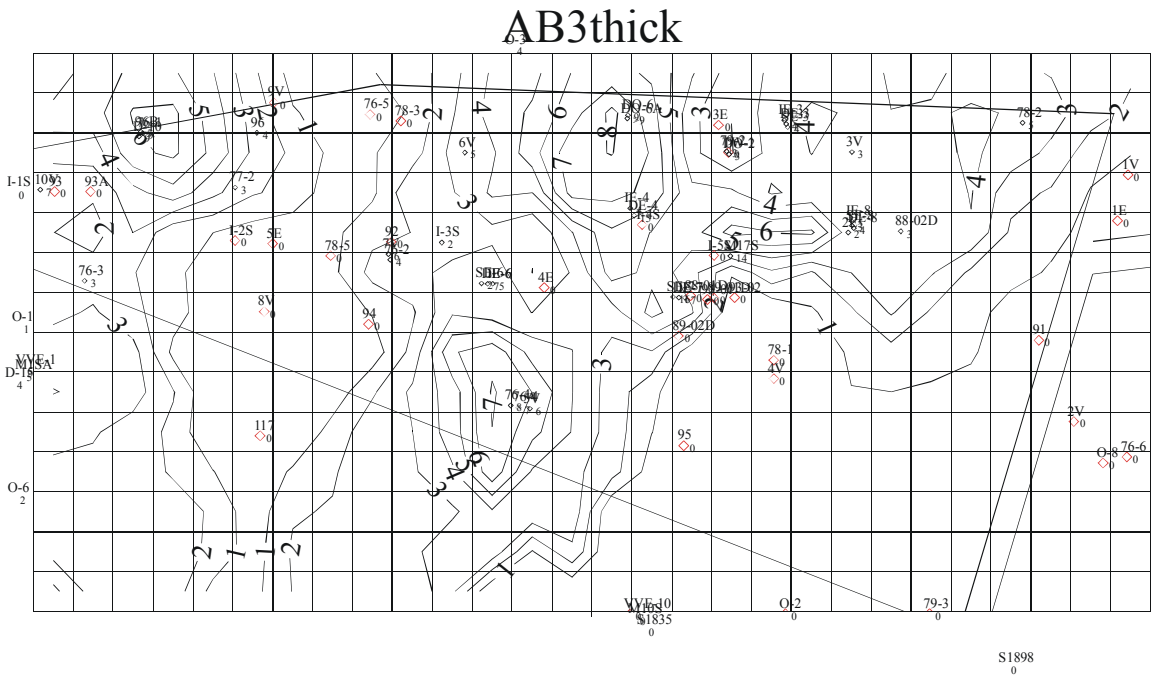

Figure B-6. Kriged A-B interbed thickness (feet) for Grid 3.

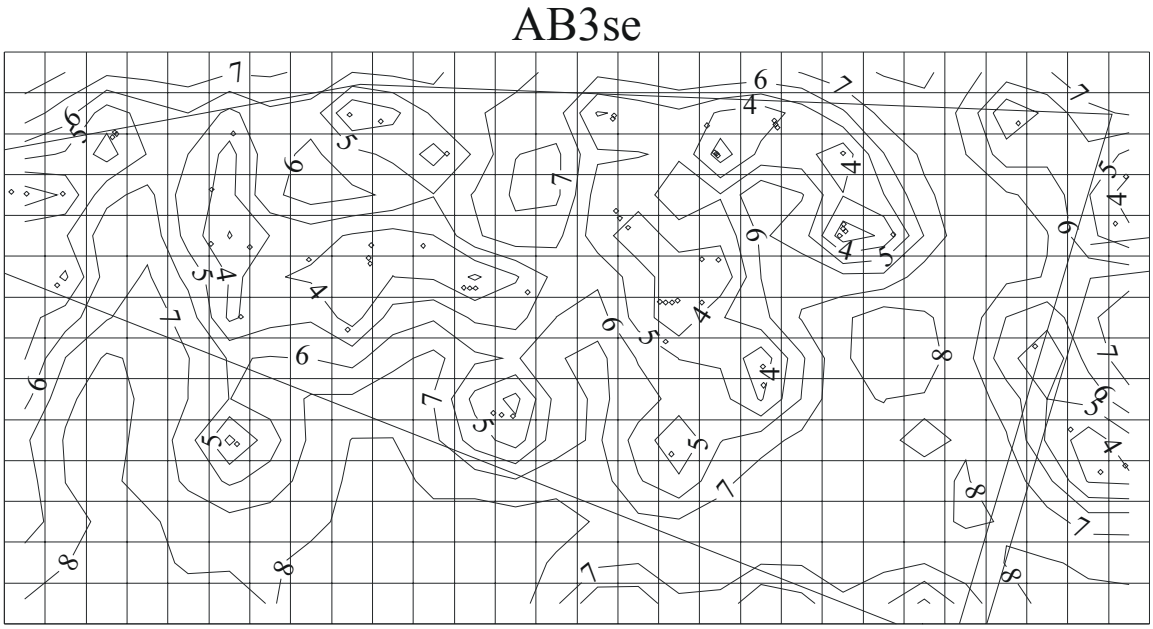

Figure B-7. Kriged A-B interbed top elevation standard error (feet) for Grid 3.

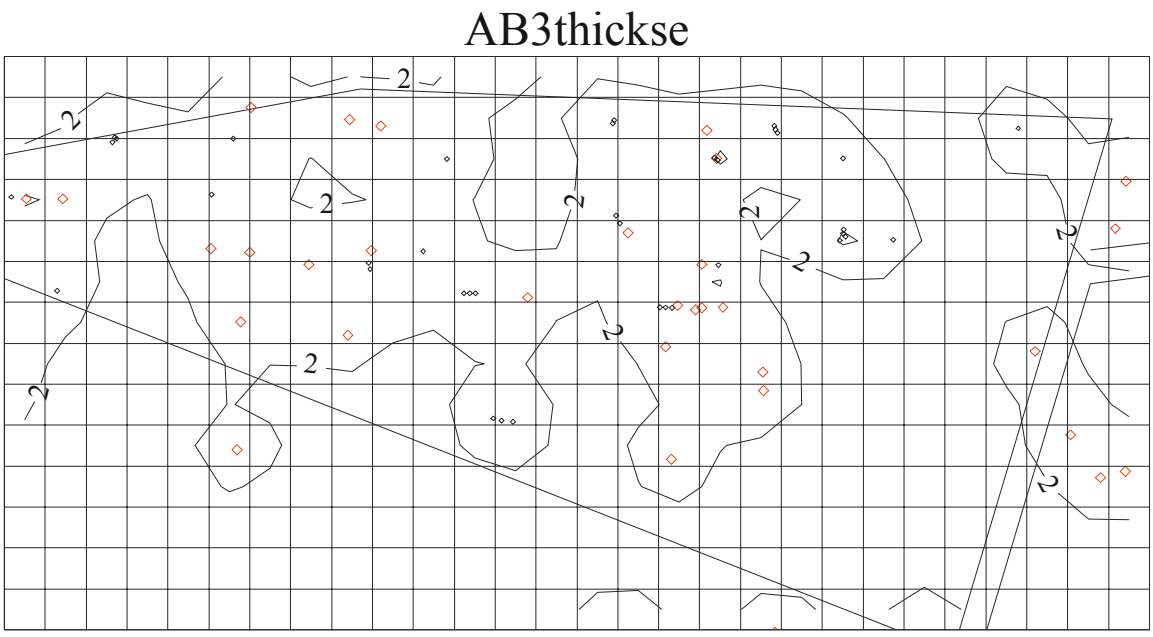

Figure B-8. Kriged A-B interbed thickness standard error (feet) for Grid 3.

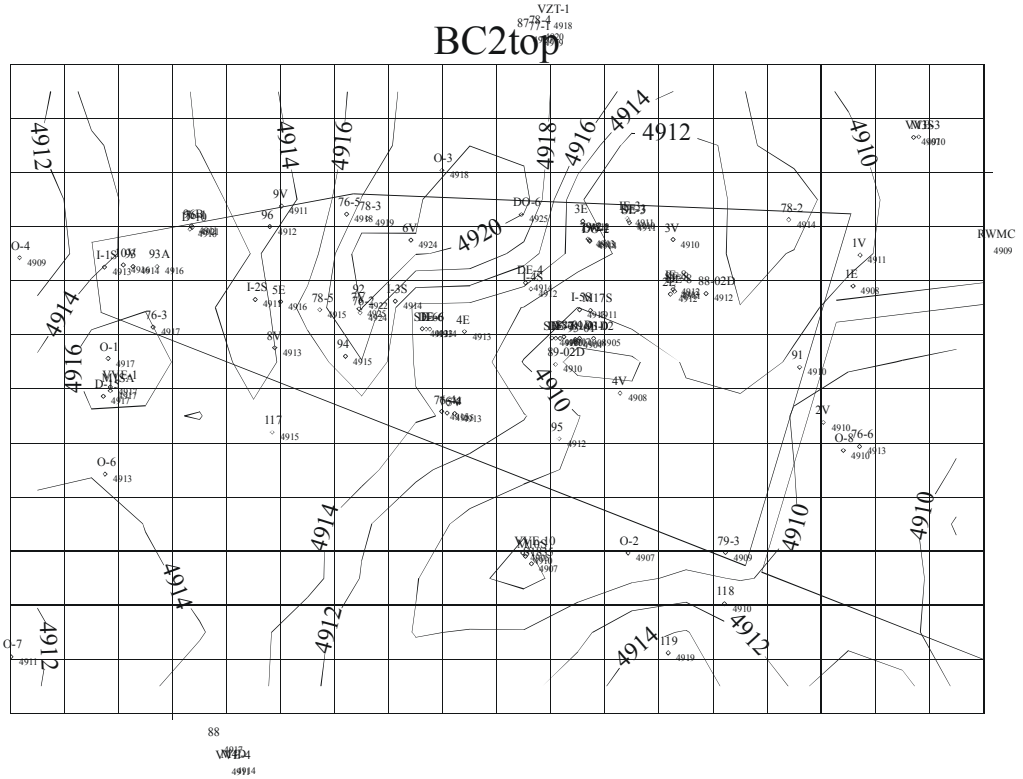

Figure B-9. Kriged B-C interbed top elevation (feet) for Grid 2.

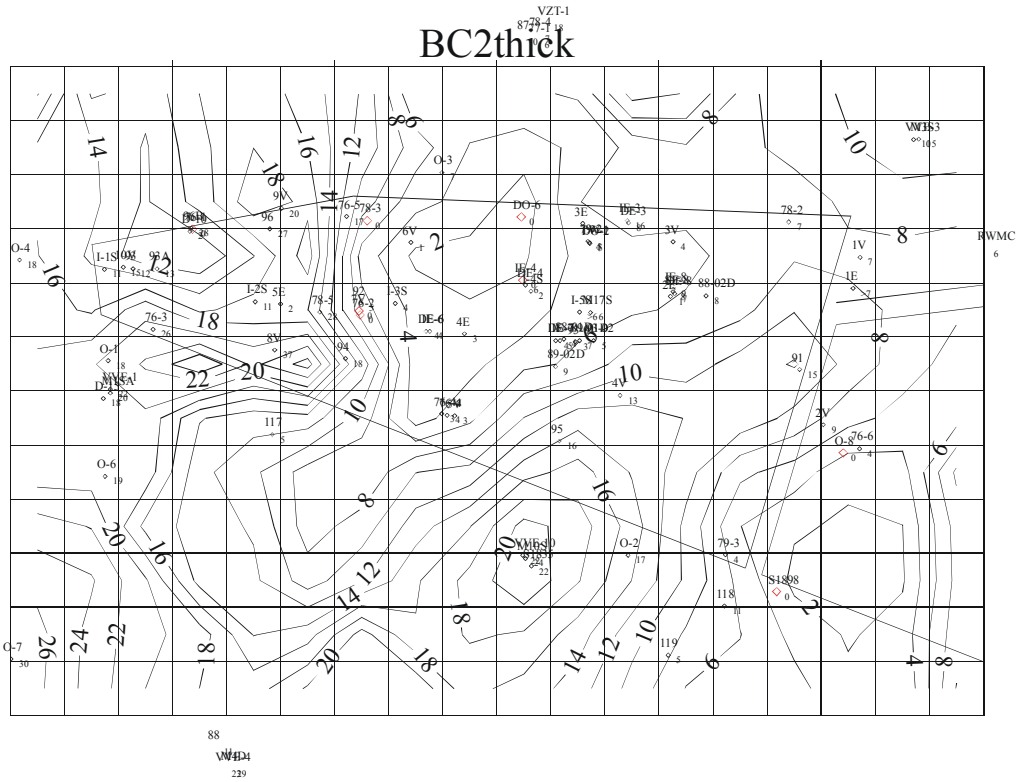

Figure B-10. Kriged B-C interbed thickness (feet) for Grid 2.

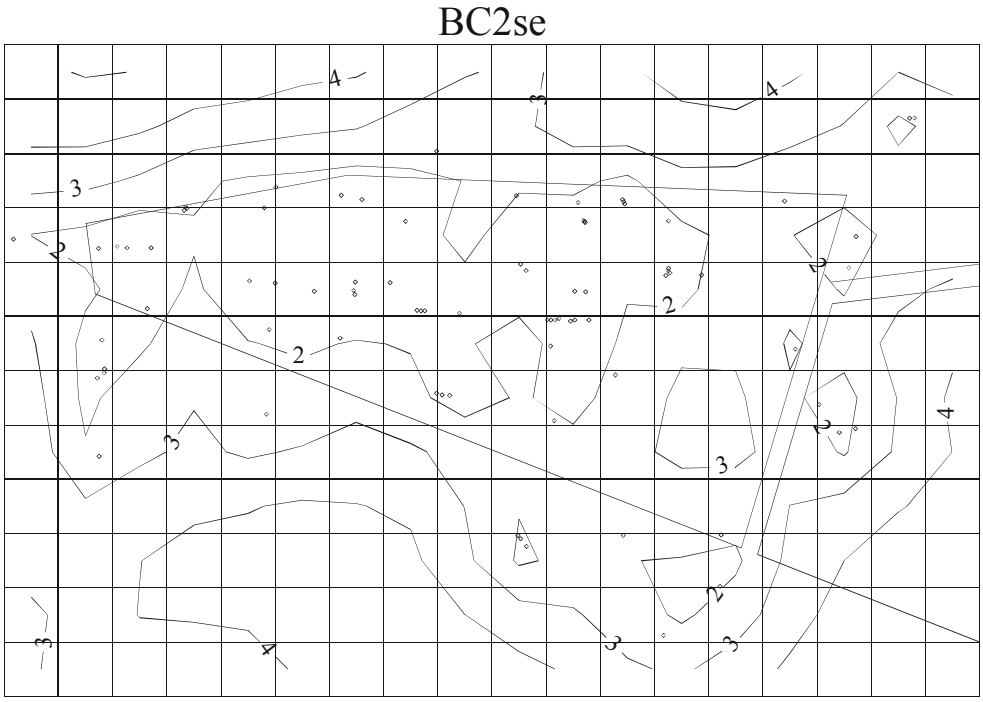

Figure B-11. Kriged B-C interbed top elevation standard error (feet) for Grid 2.

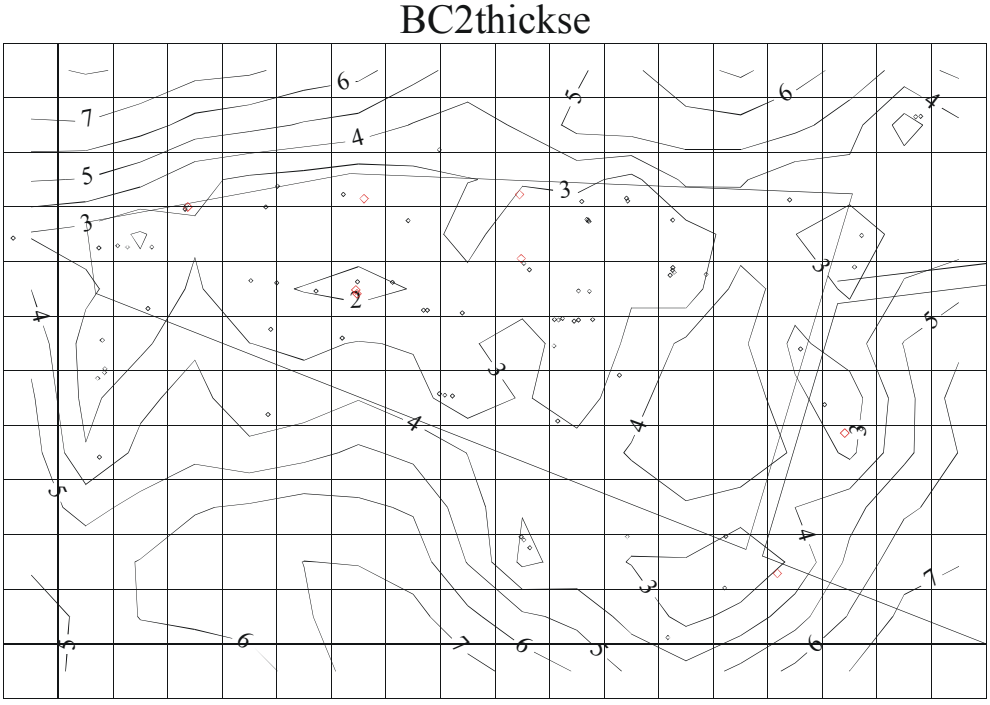

Figure B-12. Kriged B-C interbed thickness standard error (feet) for Grid 2.

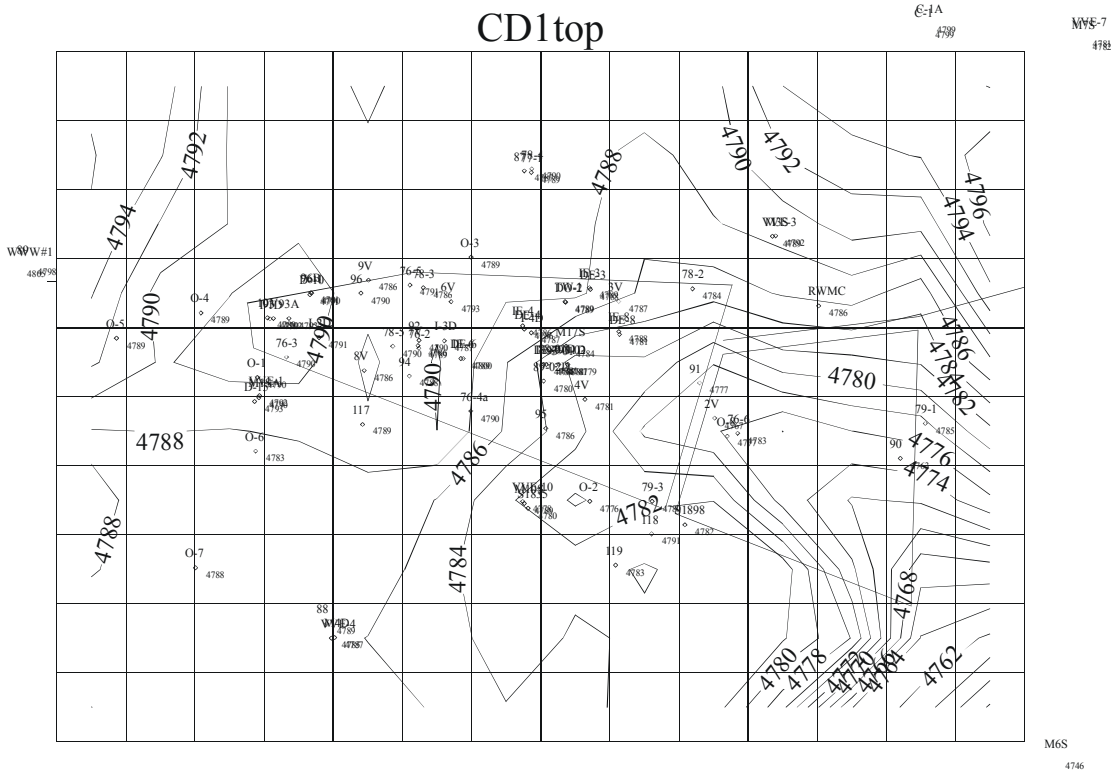

Figure B-13. Kriged C-D interbed top elevation (feet) for Grid 1.

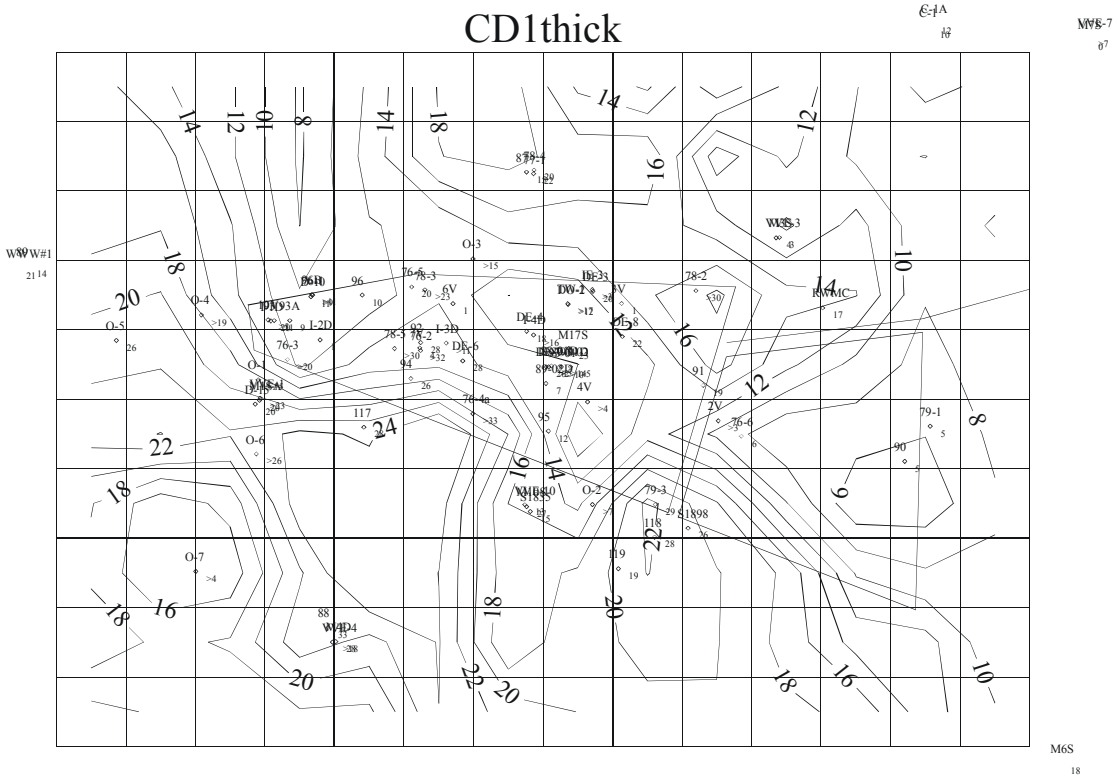

Figure B-14. Kriged C-D interbed thickness (feet) for Grid 1.

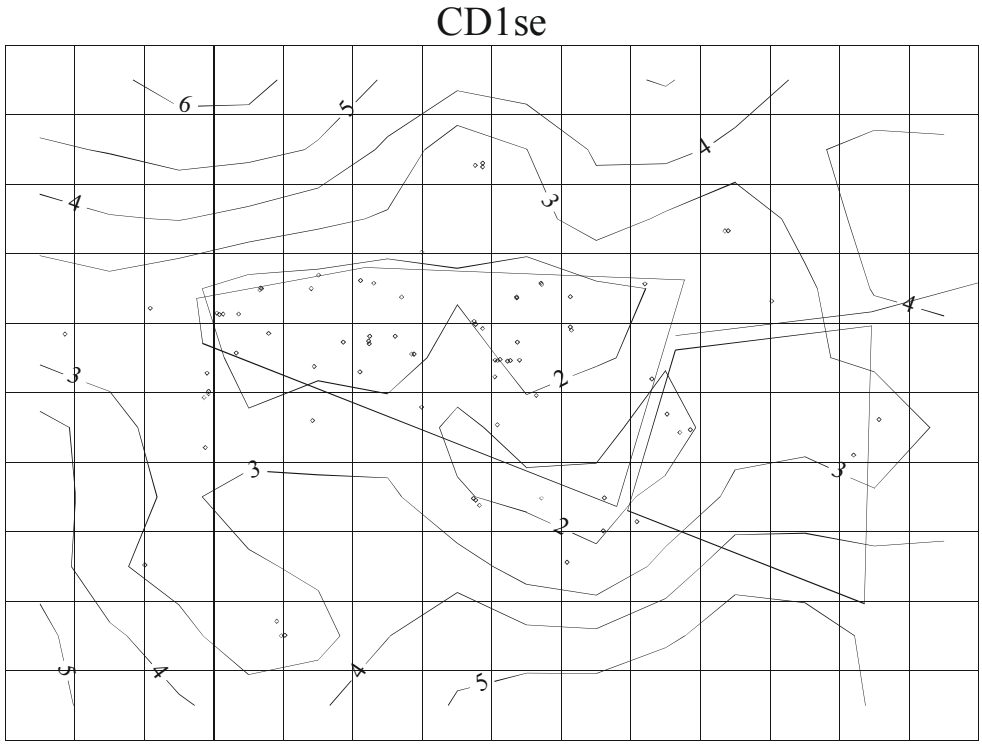

Figure B-15. Kriged C-D interbed top elevation standard error (feet) for Grid 1.

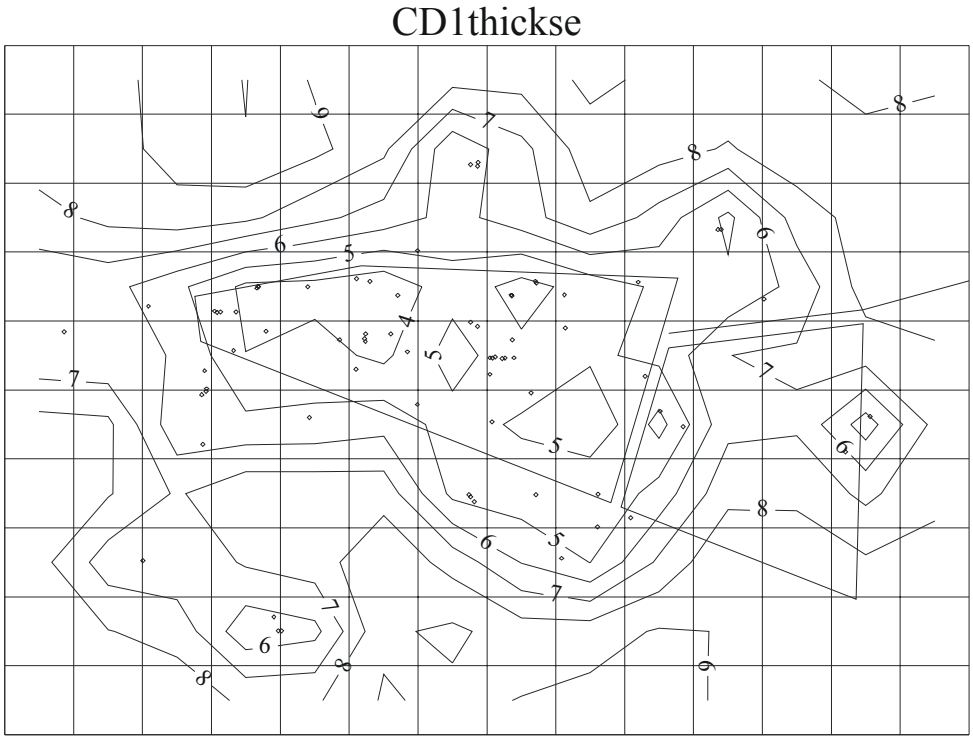

Figure B-16. Kriged C-D interbed thickness standard error (feet) for Grid 1.

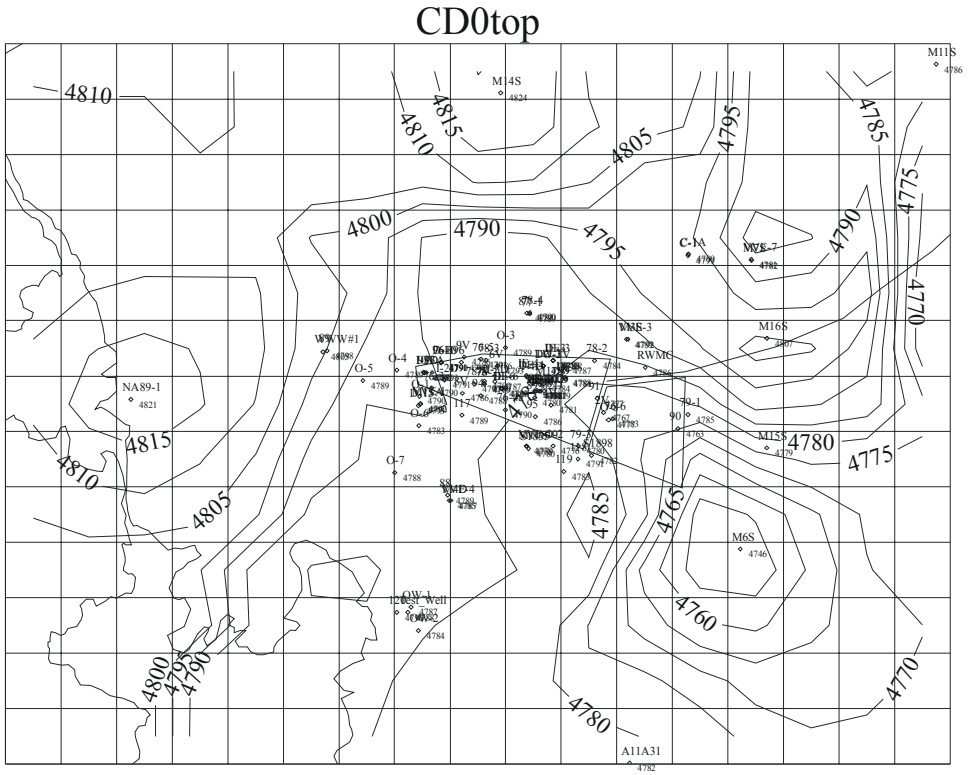

Figure B-17. Kriged C-D interbed top elevation (feet) for Grid 0.

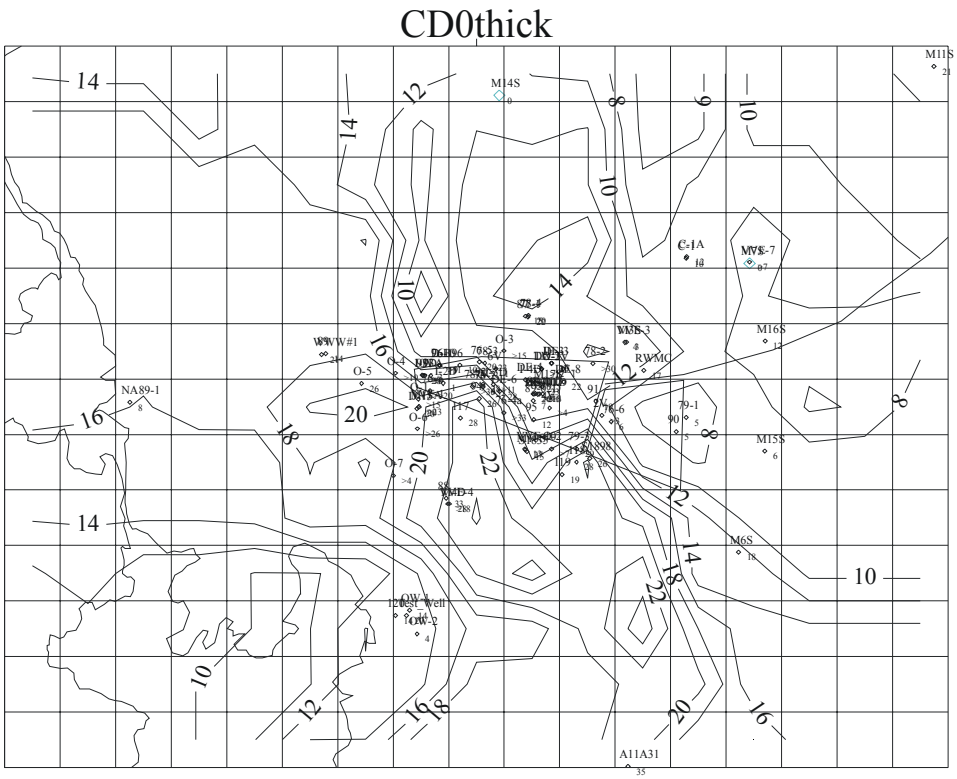

Figure B-18. Kriged C-D interbed thickness (feet) for Grid 0.

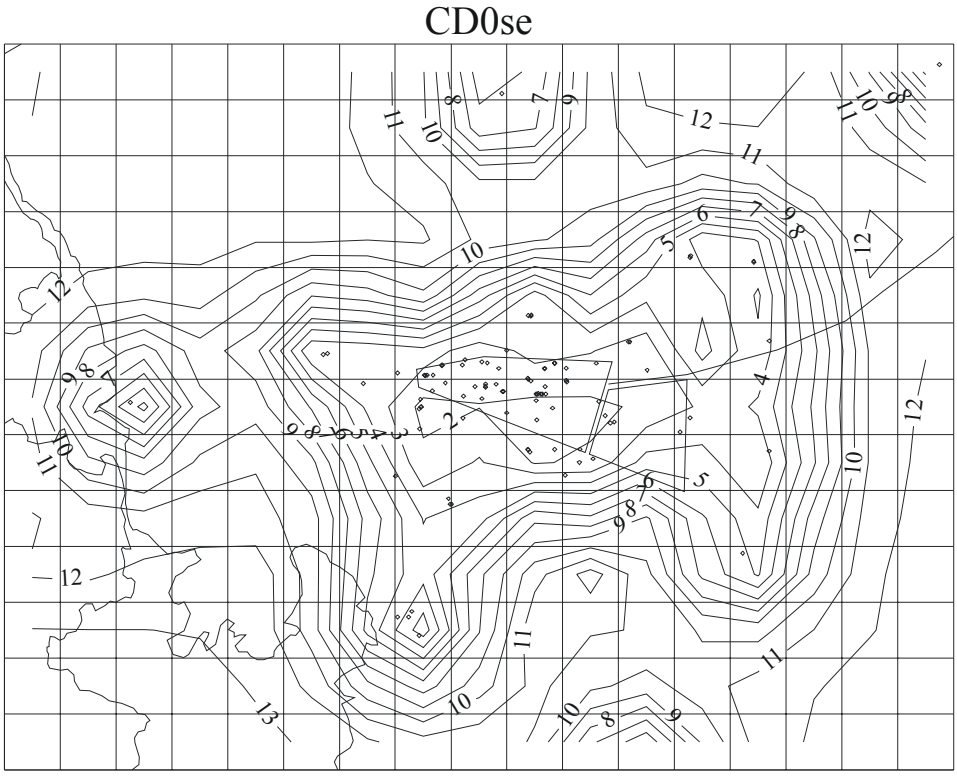

Figure B-19. Kriged C-D interbed top elevation standard error (feet) for Grid 0.

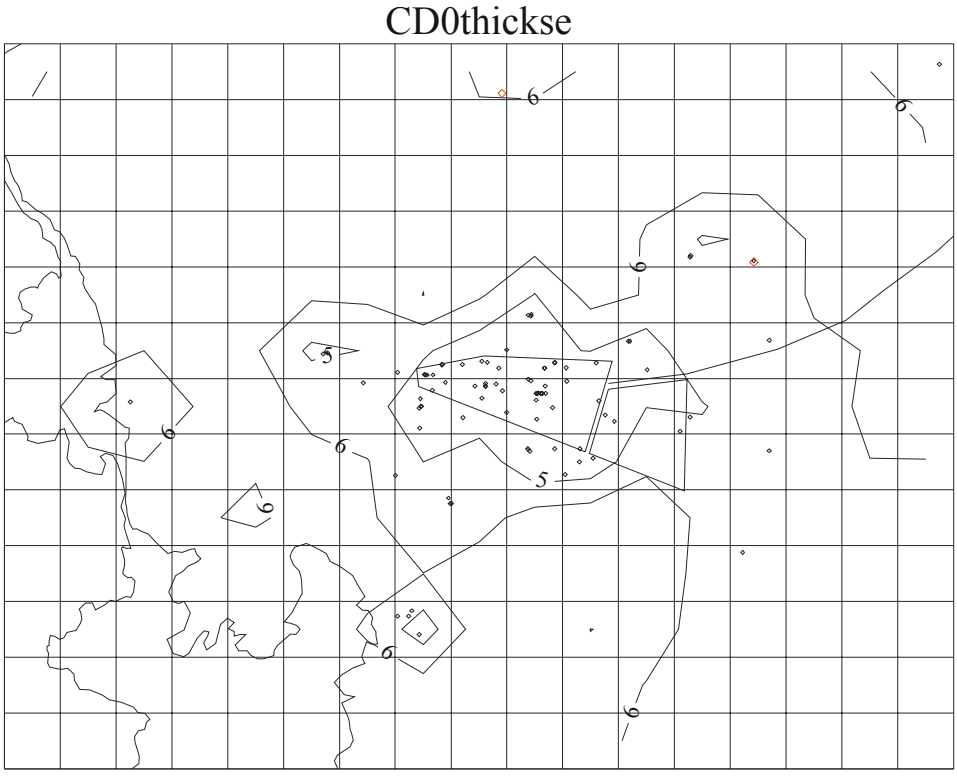

Figure B-20. Kriged C-D interbed thickness standard error (feet) for Grid 0.